© 2022. Published by The Company of Biologists Ltd | Development (2022) 149, dev200642. doi:10.1242/dev.200642

RESEARCH ARTICLE

Functional analysis of the *Vsx2* super-enhancer uncovers distinct *cis*-regulatory circuits controlling *Vsx2* expression during retinogenesis

Fuyun Bian[1], Marwa Daghsni[1], Fangfang Lu[1,2], Silvia Liu[3], Jeffrey M. Gross[1,4,5] and Issam Aldiri[1,4,5]

ABSTRACT

Vsx2 is a transcription factor essential for retinal proliferation and bipolar cell differentiation, but the molecular mechanisms underlying its developmental roles are unclear. Here, we have profiled VSX2 genomic occupancy during mouse retinogenesis, revealing extensive retinal genetic programs associated with VSX2 during development. VSX2 binds and transactivates its enhancer in association with the transcription factor PAX6. Mice harboring deletions in the *Vsx2* regulatory landscape exhibit specific abnormalities in retinal proliferation and in bipolar cell differentiation. In one of those deletions, a complete loss of bipolar cells is associated with a bias towards photoreceptor production. VSX2 occupies *cis*-regulatory elements nearby genes associated with photoreceptor differentiation and homeostasis in the adult mouse and human retina, including a conserved region nearby *Prdm1*, a factor implicated in the specification of rod photoreceptors and suppression of bipolar cell fate. VSX2 interacts with the transcription factor OTX2 and can act to suppress OTX2-dependent enhancer transactivation of the *Prdm1* enhancer. Taken together, our analyses indicate that *Vsx2* expression can be temporally and spatially uncoupled at the enhancer level, and they illuminate important mechanistic insights into how VSX2 is engaged with gene regulatory networks that are essential for retinal proliferation and cell fate acquisition.

KEY WORDS: VSX2, Chromatin, Super-enhancers, Retina, Neurogenesis, Bipolar cells, Cell fate, PAX6

INTRODUCTION

Retinal development is achieved through sequential coordinated steps that ultimately lead to the generation of seven major retinal cell types, born in a conserved order (Cepko et al., 1996; Livesey and Cepko, 2001). The initial events in retinal development involve the expansion of the retinal progenitor cells (RPCs), through multiple rounds of cell divisions, before they exit the cell cycle and give rise to six neuronal and one glial cell type (Bassett and Wallace, 2012). The transcription factors that drive proliferation and terminal differentiation often function in networks that are cell-type specific and autoregulatory in nature (Mao et al., 2008; Wang et al., 2014). Of those transcription factors, *Vsx2* is a homeodomain-containing transcription factor expressed in RPCs, and becomes restricted to retinal bipolar cells and, to a lesser extent, Müller glia (Burmeister et al., 1996; Kim et al., 2008; Liu et al., 1994; Philips et al., 2005; Rowan and Cepko, 2004, 2005). Mutations in VSX2 are associated with microphthalmia in humans and mice, impacting retinal proliferation and cell-type differentiation (Bar-Yosef et al., 2004; Burmeister et al., 1996; Ferda Percin et al., 2000; Green et al., 2003; Williamson and FitzPatrick, 2014).

Mouse studies revealed diverse roles of *Vsx2* during retinogenesis (Burmeister et al., 1996; Clark et al., 2008; Dorval et al., 2006; Green et al., 2003; Horsford et al., 2005; Liu et al., 1994; Livne-Bar et al., 2006; Rowan and Cepko, 2005; Rowan et al., 2004; West and Cepko, 2022). Loss of Vsx2 function leads to a severe reduction in retinal proliferation and a complete absence of bipolar cells (Burmeister et al., 1996; Ferda Percin et al., 2000; Green et al., 2003; Kim et al., 2008; Livne-Bar et al., 2006). VSX2 also acts to maintain neural retinal identity by repressing retinal pigment epithelium (RPE) identity via constraint of *Mitf* expression, and is implicated in suppressing rod photoreceptor differentiation in the neonatal retina (Dorval et al., 2006; Horsford et al., 2005; Livne-Bar et al., 2006; Rowan et al., 2004).

Investigation of the *Vsx2* function in postnatal mouse retina points toward a regulatory network that involves OTX2, VSX2 and PRDM1(BLIMP1) in establishing a binary cell fate decision of bipolar cells versus rod photoreceptors (Brzezinski et al., 2010; Katoh et al., 2010; Mills et al., 2017; Wang et al., 2014). *Otx2* is a homeobox transcription factor that is required for the proper genesis of photoreceptors and bipolar cells, whereas *Prdm1* is involved in the rod photoreceptor production (Brzezinski et al., 2010; Fossat et al., 2007; Goodson et al., 2020a.b; Housset et al., 2013; Katoh et al., 2010; Koike et al., 2007; Nishida et al., 2003). Data indicate that retinal precursors expressing both Otx2 and Vsx2 give rise to bipolar cells, while precursors that co-express Otx2 and Prdm1 form rod photoreceptors (Goodson et al., 2020a,b; Katoh et al., 2010; Wang et al., 2014). In this model, Prdm1 negatively regulates *Vsx2* expression, thus promoting rod cell fate by suppressing bipolar cell specification in rod precursors (Goodson et al., 2020a; Katoh et al., 2010; West and Cepko, 2022). Whether VSX2 inhibits *Prdm1* expression in bipolar cell precursors has not been established (Goodson et al., 2020a; West and Cepko, 2022). VSX2 likely exerts its function primarily by engaging with *cis*-regulatory elements (Clark et al., 2008; Reichman et al., 2010) and direct and indirect protein-protein interactions (Wilson et al., 1993). How VSX2 impinges on chromatin structure to orchestrate retinogenesis remains unclear.

Temporal and spatial control of gene expression during development is usually achieved by noncoding DNA sequences

[1]Department of Ophthalmology, University of Pittsburgh School of Medicine, Pittsburgh, PA 15213, USA. [2]Department of Ophthalmology, The Second Xiangya Hospital, Central South University, Changsha, Hunan 410011, China. [3]Department of Pathology, University of Pittsburgh School of Medicine, Pittsburgh, PA 15213, USA. [4]Department of Developmental Biology, University of Pittsburgh School of Medicine, Pittsburgh, PA 15213, USA. [5]Louis J. Fox Center for Vision Restoration, University of Pittsburgh School of Medicine, Pittsburgh, PA 15213, USA.

*Author for correspondence (aldirii@pitt.edu)

I.A., 0000-0002-0813-2943

Handling Editor: François Guillemot
Received 14 February 2022; Accepted 24 June 2022

Development (2022) 149, dev200642. doi:10.1242/dev.200642

that act distally to regulate transcription in a tissue-specific manner (Buecker and Wysocka, 2012; de Laat and Duboule, 2013). Approximately 98% of the human genome is composed of non-coding sequences, much of which are likely to have regulatory functions (Pennacchio et al., 2013). Previous studies, including ours, have identified the *cis*-regulatory landscape of retinal cells in mice and humans (Aldiri et al., 2017; Hartl et al., 2017; White et al., 2016). The challenge now is to define the intended target genes of these enhancers and to map promoter-enhancer physical interactions in the complex 3D genome during retinal development, which is essential to understanding the molecular mechanisms underlying retinal development and diseases.

We have previously identified a large *cis*-regulatory region (a super-enhancer) upstream of *Vsx2* that is required for the bipolar cell genesis (Norrie et al., 2019). However, several key important questions remained unanswered. For example, why did this enhancer deletion result in microphthalmia? What is the fate of retinal precursor cells destined to become bipolar cells? And what are the molecular mechanisms underlying the activation of *Vsx2* regulatory elements during normal development? To address these questions, we mapped VSX2 genomic occupancy during retinogenesis, revealing VSX2-associated developmental gene networks. VSX2 binds its enhancer and cooperates with PAX6 to induce its activity. We further show that deleting a small region within the *Vsx2* regulatory structure in mice impacts retinal proliferation and proper bipolar cell differentiation. We also show that retinae with a large deletion in the *Vsx2* regulatory landscape suffer an increase in photoreceptor production and elevation in the expression of the *Prdm1*. VSX2 interacts with OTX2, occupies a conserved *Prdm1* enhancer and can suppress the ability of OTX2 to activate the *Prdm1* enhancer *in vitro*. Our data provide mechanistic insights into the role of VSX2 as a predominant transcriptional effector during retinogenesis, and how it drives cell fate specification and differentiation in RPCs.

RESULTS

VSX2 genomic occupancy during mouse development

To understand the roles of VSX2 in the murine developing retina, we demarcated genome-wide VSX2-associated chromatin regions by performing ChIP-Seq at E14.5 retina, defining over 9000 binding sites (Fig. 1A; Table S1). Gene Ontology (GO) term analysis of VSX2-bound peaks using Genomic Regions Enrichment of Annotations Tool (GREAT) (McLean et al., 2010) revealed top enrichment in biological functions related to retinal neurogenesis and morphogenesis, and spinal cord development, consistent with known functions of *Vsx2* (Fig. 1C) (Clovis et al., 2016; Ferda Percin et al., 2000; Kim et al., 2008). To further delineate how VSX2 is associated with neural differentiation, we performed motif analysis of VSX2-binding sites using hypergeometric optimization of motif enrichment (HOMER) (Heinz et al., 2010). This analysis underscores an over-representation of sequences related to the binding of homeodomain-containing transcription factors, especially LIM-homeodomain (Lhx) proteins, which play predominant roles in retinal cell fate acquisition (Fig. 1B) (de Melo et al., 2016; Roy et al., 2013; Zibetti et al., 2019). Interestingly, the analysis indicates a particular enrichment in the Q50 homeoprotein consensus binding motif (TAATT$^{A}/_{G}$; Fig. 1B) (Murphy et al., 2019). Inspection of VSX2 occupancy revealed a robust presence near distinct groups of genes that regulate neural progenitor programs, including components of signaling pathways (*Sfrp2*), epigenetic regulators (*Smarca4*) and transcription factors (*Lhx2*) (Fig. 1D). Given that *Vsx2* is expressed in RPCs and the adult retina, we sought to compare VSX2-associated genome-wide profiles in these two stages. We performed ChIP-Seq on adult mouse retina, defining over 19,000 peaks (Fig. 1E-H; Table S1). Similar to the E14.5 retina, motif analysis of VSX2-binding sites indicated a prevalent sequence enrichment of the Q50 motifs, which are suggested to be associated with transcription repression in bipolar cells (Fig. 1F) (Hughes et al., 2018; Murphy et al., 2019). However, GO analysis suggests more diverse roles of VSX2 that are related to cell homeostasis (mitochondria localization) and neuronal functions (phototransduction and action potential) (Fig. 1G). Because VSX2 is primarily expressed in retinal bipolar cells in the adult retina, we examined its genomic distribution within known bipolar cell genes. The analysis revealed enrichment of VSX2 within bipolar cell signature genes (126/149; 84.6%), as illustrated for *Neurod4* and *Cabp5* (Fig. 1H, Table S2). Notably, the over-representation of biological terms related to phototransduction, a function primarily mediated by photoreceptors, suggests that photoreceptor genes are principal targets for VSX2 occupancy, in agreement with previous data (Dorval et al., 2006). Indeed, we found that 117/190 (61.6%) and 65/108 (60.2%) of rod and cone genes, respectively, contained VSX2 peaks, including *Pde6c* (cones), and *Crx*, *Tulp1* and *Rbp3* (rods) (Fig. 1H,J; Table S2). This finding is consistent with the hypothesis that VSX2 maintains retinal bipolar cell identity by directly repressing non-bipolar gene expression programs, including those related to photoreceptors, in bipolar cells (Dorval et al., 2006; Livne-Bar et al., 2006; Murphy et al., 2019).

We then compared VSX2 genome binding profiles in E14.5 and adult retina. Data indicate that VSX2-shared peaks represent 33% (3077/9083) and 16% (3077/19,025) of E14.5 and adults peaks, respectively, indicating that VSX2 genomic binding profiles in RPCs and postmitotic neurons are largely non-overlapping (Fig. 1I, Table S1). Among VSX2-binding sites that are common between E14.5 and adult retina are those related to nearby genes known to be expressed in the developing and adult retina, such as *Notch1*, *Dkk3* and *Isl1* (Fig. 1J). The VSX2 preferential binding profile in adult retina includes photoreceptor and bipolar gene signatures, as described above (Fig. 1H,J), whereas E14.5-specific sites are associated with genes that are implicated in early retinal differentiation programs, such as *Neurog2* and *Olig2* (Fig. 1J). We also noticed evidence of VSX2 occupancy of nearby genes not expressed in the retina and known to be upregulated at E14.5 upon loss of *Vsx2* function, such as *Tfec* (Fig. 1J, discussed later), likely reflecting direct transcriptional repression mediated by VSX2 (Fig. 1J). Taken together, our analysis reveals distinct networks of genes regulated by VSX2 in the developing and adult retina, underscoring the diverse roles that *Vsx2* plays in establishing proper transcriptional programs of retinal lineage fate commitment.

An autoregulatory loop governs *Vsx2* expression during retinogenesis

We noticed that VSX2 robustly binds conserved non-coding regions upstream of *Vsx2* itself (termed EN1 and EN2 hereafter) in E14.5 and adult retina (Fig. 2A). When explored with our previously published E14.5 retinal epigenomic data (Aldiri et al., 2017), these areas have sharp ATAC-Seq peaks, rich in enhancer marks such as BRD4 and H3K4me1, and are occupied by RNA polymerase II (RNAPII), which is indicative of enhancer activities (Fig. 2A). We reasoned that VSX2 modulates its enhancer through a positive-feedback loop. To test this, we performed luciferase assays in 293T cells, transfecting plasmids with or without Vsx2 cDNA along with luciferase vectors containing EN1 or EN2 fragments. Indeed, VSX2

Development (2022) 149, dev200642. doi:10.1242/dev.200642

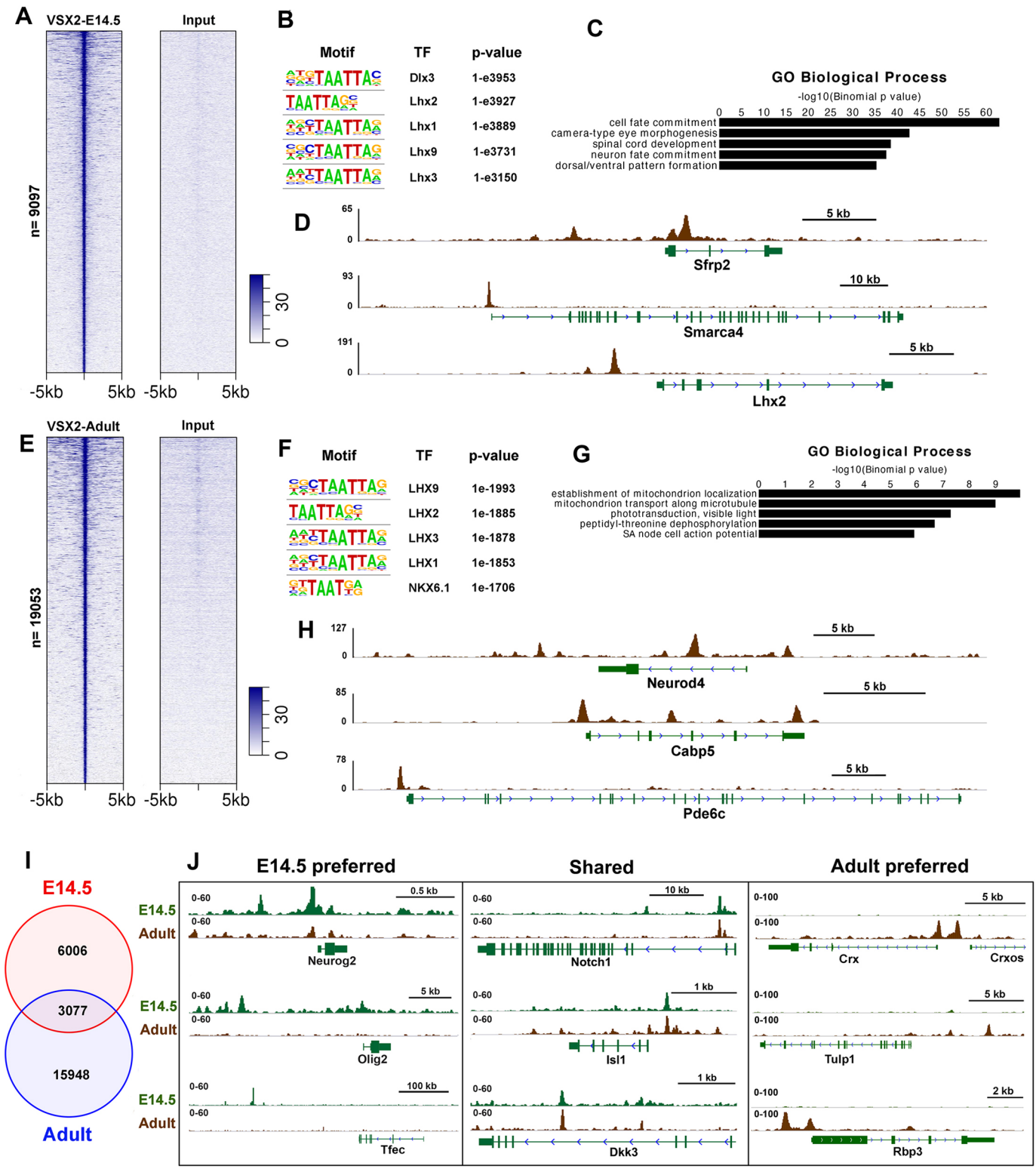

Fig. 1. VSX2 genome-wide occupancy during retinal development. (A-D) VSX2 ChIP-Seq analysis on E14.5 mouse retina. (A) Heatmaps of ChIP-Seq binding signal intensity (plotted within 10 kb window around the peak center) for VSX2 and input. (B) Top five motifs enriched within VSX2 peak summits at E14.5 retina. (C) Top five significantly enriched Gene Ontology (GO) terms of biological processes of VSX2-bound peaks at E14.5, as analyzed by GREAT. (D) Genome browser snapshots of E14.5 VSX2 peaks nearby the RPC genes *Sfrp2* (signaling), *Smarca4* (chromatin regulation) and *Lhx2* (transcription regulation). (E-H) VSX2 ChIP-Seq analysis on adult mouse retina. (E) Heatmap of ChIP-Seq binding signal intensity for VSX2 and input within ±5 kb of peak center. (F) Motif analysis of VSX2-binding regions in the adult retina (top five enrichment terms are shown). (G) GO enrichment analysis of VSX2 peaks. (H) VSX2 ChIP-Seq tracks near *Neurod4* and *Cabp5* (bipolar cells), and Pde6C (cones). (I) Venn diagram showing overlapping VSX2-binding regions shared between E14.5 and adult retina. (J) Example VSX2-binding sites of the E14.5-preferred, shared and adult-preferred sites.

Development (2022) 149, dev200642. doi:10.1242/dev.200642

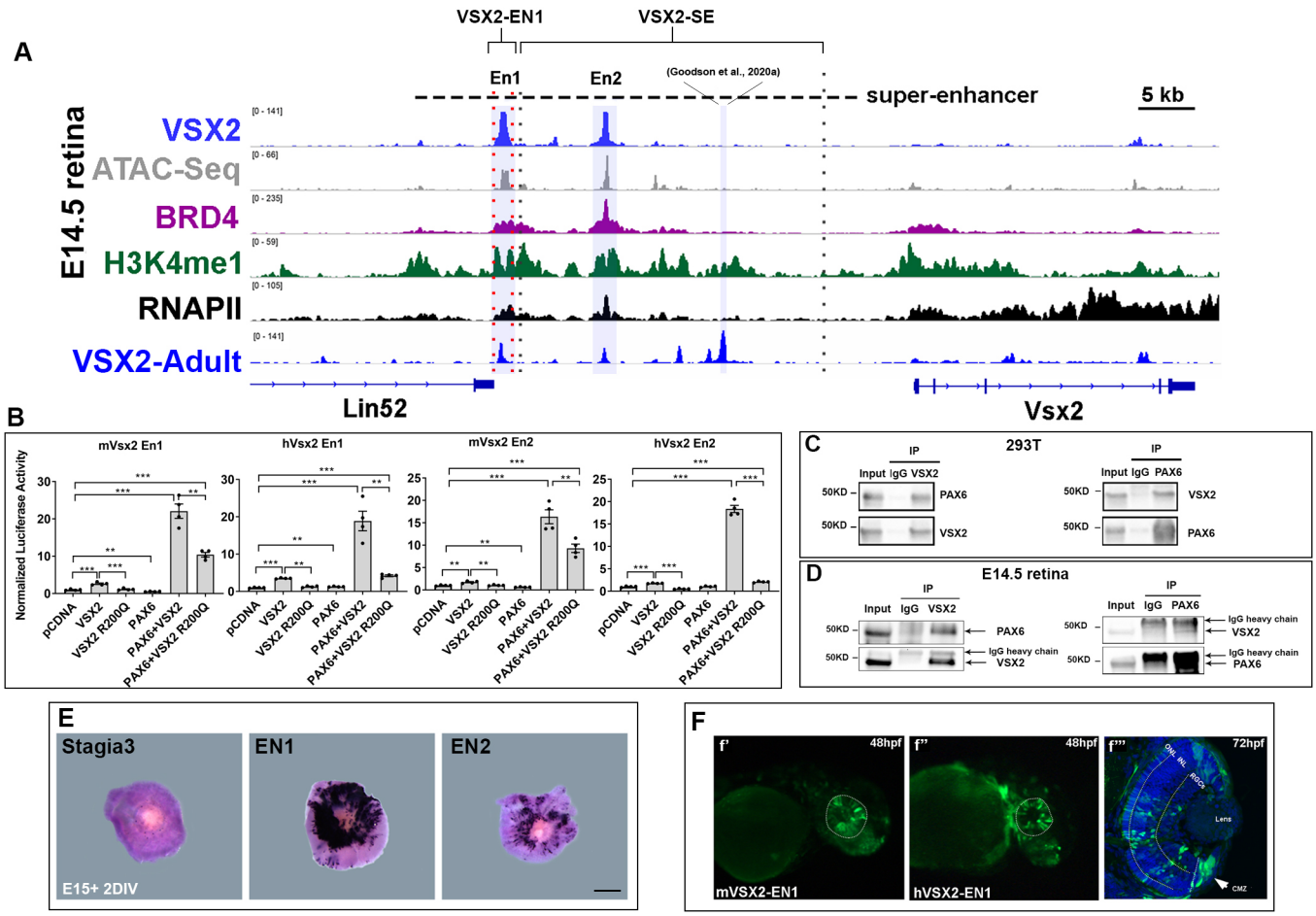

Fig. 2. An autoregulatory loop governs *Vsx2* expression during retinogenesis. (A) The chromatin landscape near Vsx2 in E14.5 retina, as revealed by ATAC-Seq, BRD4, H3K4me1 and RNAPII occupancy (ChIP-Seq data from Aldiri et al., 2017), and the binding of VSX2 in E14.5 and adult retina. The relative genomic site of the putative super-enhancer (dotted line) and mouse knockout borders are shown. The positions of EN1, EN2 and a recently reported enhancer (Goodson et al., 2020a) are highlighted in light gray. (B) Luciferase assays of mouse and human EN1 and EN2 in the presence of VSX2, VSX2 (R200Q) and/or PAX6. Data are mean±s.e.m., n=4. ***P<0.001; **P<0.01; two-tailed unpaired Student's t-test (C,D) Co-IP assay performed on cell lysates of transfected 293T cells (C) and E14.5 retina (D) showing the interaction of VSX2 and PAX6. The antibodies used for immunoprecipitation and western blotting are indicated above and to the right of the panels, respectively. 5% input was used. Arrows highlight the position of the IgG heavy chain recognized by the antibody versus true protein band. (E) AP activity of the *Vsx2* enhancer elements EN1 and EN2 cloned in the Stagia3 reporter construct and electroporated in the developing mouse retinas. Scale bar: 500 µm. (F) Representative images of zebrafish embryos injected with mouse (f′) or human (f″) VSX2-EN1 constructs. f‴ is a retinal cross-section at 72 hpf. The CMZ proliferative area is highlighted by an arrow.

can significantly transactivate mouse and human EN1 and EN2 elements in 293T cells (Fig. 2B). Earlier work identified a point mutation (R200Q) in the VSX2 homeodomain that is associated with microphthalmia in humans (Ferda Percin et al., 2000), impairing the ability of VSX2 to bind DNA (Zou and Levine, 2012), and human retinal organoids carrying this mutation suffer from reduced retinal growth and loss of bipolar cells (Phillips et al., 2014). Transfection of Vsx2 harboring the R200Q point mutation led to a sharp decrease in the VSX2-dependent enhancer activities (Fig. 2B). We reasoned that VSX2 binds EN1 and EN2 through discrete motif sequences in its regulatory elements. Our earlier work defined a VSX2 consensus motif in EN2 (Norrie et al., 2019), but a recent study indicated that this motif is dispensable for *Vsx2* expression (Honnell et al., 2022). Thus, we focused on EN1 and defined three sites with the homeodomain recognition motif (TAATTA) that overlap with the VSX2 ChIP-Seq peak (Fig. S1A). A minimal EN1 enhancer constituent (165 bp) containing motif 2 (CTCTAATTAG) lies at the peak center and is sufficient to drive luciferase activity in the presence of VSX2, whereas a deletion in this sequence diminished EN1 enhancer activity (Fig. S1B).

Given earlier studies suggesting that VSX2 can bind to homeodomain-containing transcription factors, we hypothesized that VSX2 may cooperate with other transcription factors expressed in RPCs to promote its expression (Mikkola et al., 2001; Wilson et al., 1993). One such factor is PAX6, which has been implicated in the regulation of *Vsx2*, as loss of *Pax6* leads to a significant downregulation of *Vsx2* in the mouse developing retina (Farhy et al., 2013). We first tested whether PAX6 alone can activate *Vsx2* enhancers in luciferase assays and found no evidence for such a function (Fig. 2B). However, the introduction of both Vsx2 and Pax6 led to a multi-fold increase in EN1 and EN2 enhancer activities when compared with transfection of Vsx2 alone, underscoring a synergistic relationship between VSX2 and PAX6 on the *Vsx2* enhancer (Fig. 2B). Moreover, transfection of Vsx2 harboring the R200Q point mutation, in combination with Pax6, led to a sharp decrease in VSX2-dependent EN1 and EN2 enhancer activities (Fig. 2B).

Development (2022) 149, dev200642. doi:10.1242/dev.200642

Reasoning that VSX2 and PAX6 interact, we performed co-immunoprecipitation (co-IP) assays in 293T cells and E14.5 retina, and found a robust physical association (Fig. 2C,D). Together, these data suggest that PAX6 functions as a modulator to promote VSX2-dependent transcriptional activation and support the presence of a transcriptional autoregulatory loop, whereby VSX2 governs its expression in RPCs, and likely bipolar cells, in association with transcription factors important for retinal development.

Functional analyses of *Vsx2* enhancer constituents during neurogenesis

Next, we assessed the functional relevance of EN1 and EN2 in the mouse retina. We cloned EN1 and EN2 sequences into a vector (Stagia3) that contains a bicistronic reporter gene cassette (GFP-IRES-PLAP) driven by a minimal promoter (Billings et al., 2010). We then *ex vivo* electroporated wild-type E15 retina with EN1, EN2 or empty Stagia3 plasmids along with a CAG-mCherry vector as a control for electroporation efficiency (Emerson and Cepko, 2011). We cultured the retinae for 2 days and performed AP staining afterwards. Both EN1 and EN2 fragments produced robust AP activity, suggesting that they can function as regulatory enhancers in the developing mouse retina (EN1=8/8, EN2=8/8, Stagia3 empty vector=0/6; Fig. 2E, Fig. S1C). To experimentally test whether the *Vsx2* regulatory elements EN1 and EN2 are functionally conserved *in vivo*, we cloned EN1 and EN2 with GFP as a reporter gene using the Tol2kit protocol (Kwan et al., 2007), and injected the constructs into zebrafish embryos at the one-cell stage. We found that the human and mouse EN1 exhibited enhancer activities in developing zebrafish eyes (37%, n=245 for mouse EN1; 59%, n=192 for human EN1; Fig. 2F and Fig. S1D-Q), while EN2 sequences lacked activity. In retinal sections from 72 h post-fertilization (hpf) zebrafish embryos, GFP expression was observed across retinal neurons, particularly in the inner nuclear layer (INL), while the presence of GFP-positive cells in the retinal outer nuclear layer (ONL) and retinal ganglion cells (RGCs) likely resulted from EN1 enhancer activities in early RPCs (Fig. 2F and Fig. S1P,Q). Importantly, EN1 activities were also detected in the proliferative domain (ciliary marginal zone; CMZ), consistent with the known expression of *Vsx2* during zebrafish retinogenesis (Fig. 2F and Fig. S1P,Q) (Vitorino et al., 2009).

Based on these data and on our evolutionary analysis (see below), we decided to focus on testing the requirement of EN1 for *Vsx2* expression and retinal development *in vivo*. We generated a mouse enhancer knockout that harbors EN1 deletion (termed VSX2-EN1 hereunder; Fig. 2A; Fig. S2A) using CRISPR/Cas9 technology (see Materials and Methods). Mice lacking the EN1 element exhibited a severe reduction in eye size at E14.5, recapitulating ocular defects associated with *Vsx2* gene mutations (Fig. 3A) (Ferda Percin et al., 2000). To test whether EN1 is required for *Vsx2* expression, we immunostained the developing retina at various stages (E14.5, P0, P4, P7 and P10) with VSX2 antibody and found a pronounced reduction in staining signal (Fig. S2B). To address whether loss of EN1 segment influenced retinal proliferation, we performed EdU labeling coupled with mitotic Ki67 immunostaining at E14.5 and found a strong reduction in both markers, particularly in the retina periphery (Fig. 3B). Moreover, the retinal proliferation defect is associated with the presence of excessive pigmented cells at the retinal periphery (Fig. 3C), consistent with deficiencies observed upon loss of *Vsx2* function in *Orj* mice, and suggesting an essential role for EN1 enhancer in promoting retinal proliferation and suppressing RPE acquisition (Ferda Percin et al., 2000; Rowan et al., 2004). To better define the molecular defects resulting from loss of the EN1 enhancer constituent, we performed bulk RNA-Seq analysis on retinas at E14.5 (four replicas) and defined 1434 and 1577 transcripts that are downregulated and upregulated, respectively (>1.5-fold change; P-value <0.05) (Fig. 3D; Table S3). GO analysis of deregulated genes using the database for annotation, visualization and integrated discovery (DAVID) (Dennis et al., 2003) underscored a significant enrichment of biological functions related to neurogenesis and morphogenesis (Fig. S3A,B). As expected, *Vsx2* was significantly downregulated along with genes related to retinal patterning (i.e. *Vax2*), proliferation (i.e. *Ccnd1*), differentiation (i.e. *Ascl1* and *Ptf1a*) and signaling (i.e. *Hhip*, *Gli1* and *Dll3*) (Fig. 3D). Genes that were significantly upregulated include *Mitf* (hence, pigmented cell expansion), *Tfec* and *Cdkn1c*, all of which have been reported previously to be robustly induced upon loss of *Vsx2* function (Fig. 3D; Table S3) (Rowan et al., 2004).

We then investigated genetic programs that are directly regulated by VSX2 at E14.5. We incorporated RNA-Seq data from the VSX2-EN1 enhancer knockout with the VSX2 genomic profile at E14.5, revealing that 33.8% (1019/3016) of deregulated genes are associated with VSX2 occupancy, with a slight preference towards downregulated transcripts [(37% (535/1434) versus 30.6% (483/1577) of upregulated genes] (Fig. 3E-H; Table S3). Overall, these results demonstrate that the EN1 enhancer element is essential for *Vsx2* expression, retinal proliferation and the proper expression of RPC neural differentiation programs.

Differential requirements of *Vsx2* enhancer elements to retinal development

We previously generated a large deletion in the *Vsx2* regulatory landscape (termed VSX2-SE hereafter; Fig. 2A; Fig. S2A) that exhibits a complete loss of bipolar cells (Fig. 4A) (Norrie et al., 2019). This deletion includes elements important for bipolar cell differentiation (Goodson et al., 2020a) as well as EN2, but excludes the EN1 enhancer region (Fig. 2A). Unlike VSX2-EN1 enhancer knockout, loss of VSX2-SE did not affect eye size during embryogenesis or adulthood, suggesting that RPC proliferation was not impacted (Fig. S3C) (Norrie et al., 2019). To test this directly, we performed EdU labeling along with Ki67 immunostaining at E14.5 VSX2-SE retinae and found no evidence for aberrations in EdU incorporation or Ki67 staining (Fig. 3I). Still, VSX2 immunolabeling of the developing retina at stages E14.5, P0, P4, P7 and P10 suggests that VSX2 expression was impacted (Fig. S2B). Western blotting indicated a ∼35% reduction in VSX2 protein levels in the developing VSX2-SE$^{-/-}$ retinae at E14.5 when compared with a ∼90% drop in the adult retina, suggesting that *Vsx2* expression is moderately affected in RPCs but not as strongly as in the VSX2-EN1 knockout retinae (Fig. 3J). To corroborate these results and assess transcriptional programs impacted in E14.5 VSX2-SE retinae, we performed bulk RNA-Seq (three replicas). Limited changes in gene expression in comparison with VSX2-EN1 knockout were detected (59 and 151 transcripts were downregulated and upregulated, respectively), mostly impacting genes associated with generic metabolic responses and protein biogenesis functions (Table S4). Nonetheless, some interesting genes were affected, including *Mitf*, a known target for *Vsx2* repression, and *Pou2f1*, a transcription factor implicated in cone photoreceptor genesis, both of which are occupied by VSX2 (Fig. 3H,K) (Javed et al., 2020). *Vsx2* was downregulated by around 40%, yet this was insufficient to impact the expression of proliferation and cell cycle genes, consistent with

Development (2022) 149, dev200642. doi:10.1242/dev.200642

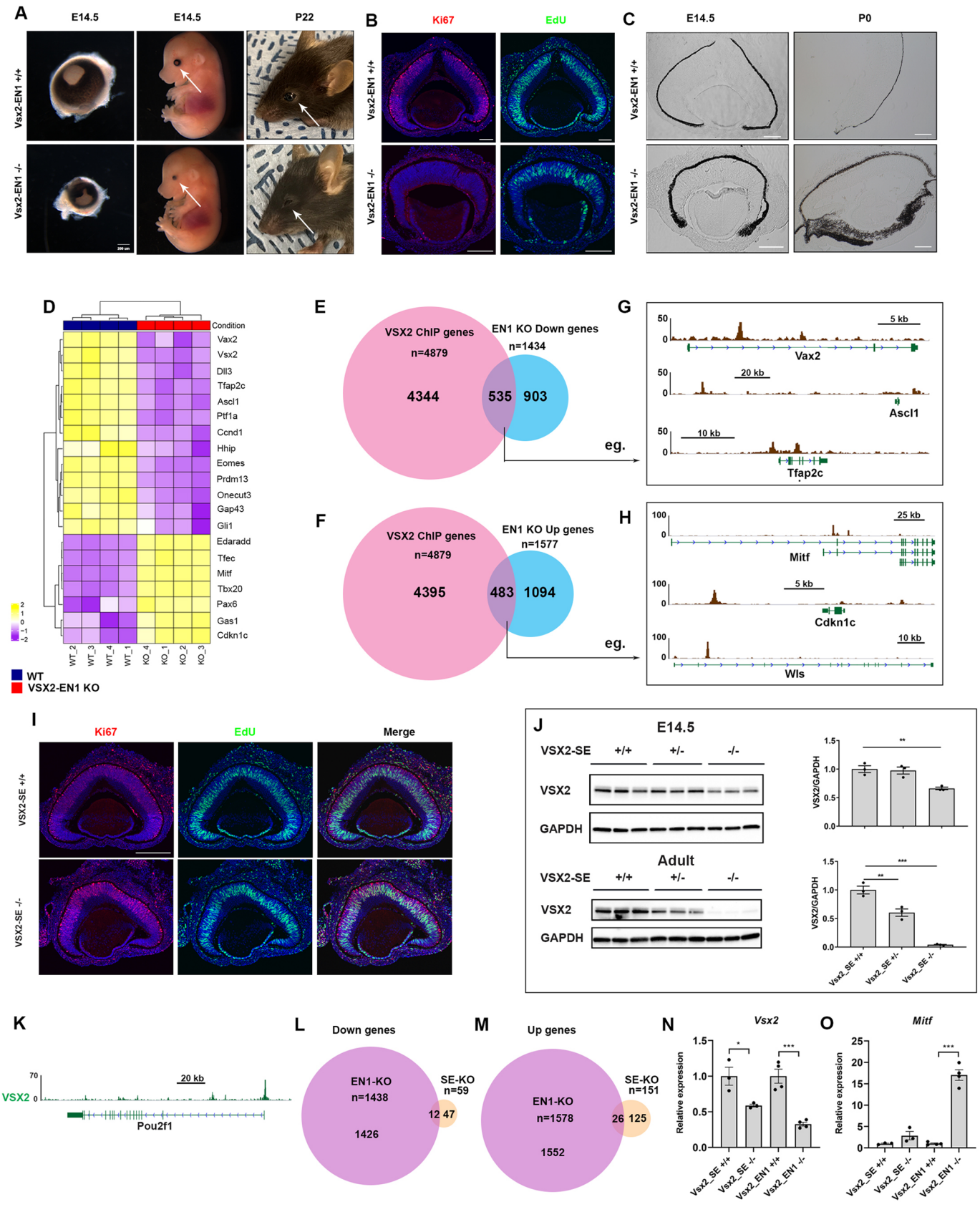

Fig. 3. See next page for legend.

Development (2022) 149, dev200642. doi:10.1242/dev.200642

Fig. 3. Analyses of VSX2 enhancer deficient retina at E14.5. (A) VSX2-EN1 knockout eyes (lower panel) are visibly micro-ophthalmic (arrows) compared with wild type (upper panel) at E14.5 and in adulthood. Arrows indicate the eye position. Scale bar: 200 µm (B) EdU incorporation and concomitant immunolabeling with Ki67 at E14.5 of wild-type (upper panel) and VSX2-EN1$^{-/-}$ retinas (lower panel) indicates reduced staining for both markers, particularly in the peripheral region. Scale bars: 100 µm. (C) VSX2-EN1 KO mice showed increased pigmentation at E14.5 and P0. Scale bars: 100 µm. (D) Heatmap of selected differentially expressed genes between wild-type and VSX2-EN1 enhancer knockout unveiled by RNA-Seq analysis. (E,F) Venn diagram showing the overlap of genes bound by VSX2 and significantly downregulated (E) and upregulated (F) in VSX2-EN1 knockout retina at E14.5. (G,H) Examples of downregulated (G) and upregulated (H) genes bound by VSX2 in E14.5 retina. (I) EdU incorporation coupled with Ki67 immunolabeling at E14.5 in wild type and VSX2-SE knockout retina showing no obvious changes in both markers. Scale bar: 200 µm. (J) Western blot analysis and quantification of VSX2 protein level in VSX2-SE KO and wild-type retina. The relative expression is shown by normalizing to GAPDH (data are mean±s.e.m., n=3; ***P<0.001; **P<0.01; two-tailed unpaired Student's t-test). (K) VSX2 occupancy profile near Pou2f1 in mouse retina at E14.5. (L,M) Venn diagram showing the overlap between downregulated (L) or upregulated (M) genes in VSX2-EN1$^{-/-}$ and VSX2-SE$^{-/-}$ retina at E14.5. (N,O) Quantification of *Vsx2* (N) and *Mitf* (O) RNA level (as determined by RNA-Seq) in VSX2-SE$^{-/-}$ and VSX2-EN1 E14.5 retinas normalized to their respective wild-type control (data are mean±s.e.m., n=3; ***P<0.001; *P<0.05; two-tailed unpaired Student's t-test).

EdU incorporation data (Fig. 3N; Fig. S3D and Table S4). We also compared the retinal transcriptomes of VSX2-SE and VSX2-EN1 knockouts at E14.5 and found little overlap (38 genes in total; Fig. 3L,M; Table S4). Notably, RNA-Seq data indicated that whereas the increase in *Mitf* expression was 15-fold in VSX2-EN1 deficient retinae, VSX2-SE retinae exhibit only a twofold change; hence, no obvious pigmentation phenotype was observed in VSX2-SE knockout retina (Fig. 3N,O). Together, these data underscore the differential requirements for *Vsx2* enhancer constituents in its expression and suggest highly specialized non-redundant functions of the *Vsx2* enhancer structure during retinogenesis.

Cell fate defects in *Vsx2* enhancer deficient retinae

We then examined the effect of deleting *Vsx2* enhancer elements on retinal cell fate acquisitions. We have previously shown that VSX2-SE knockout completely lost retinal bipolar cells, as indicated by the absence of OTX2 in the inner nuclear layer of the adult retina (Fig. 4A) (Norrie et al., 2019). However, immunostaining against VSX2 revealed the presence of a residual expression in VSX2-SE$^{-/-}$ retinae that completely overlapped with the Müller glia marker SOX9, demonstrating that this enhancer element is dispensable for *Vsx2* expression in Müller glia (Fig. 4A).

Previous work has suggested that *Vsx2* inhibits photoreceptor differentiation; our data indicate widespread occupancy of VSX2 on rod and cone genes (Fig. 1H,J) (Livne-Bar et al., 2006). Thus, we postulated that loss of *Vsx2* in the VSX2-SE$^{-/-}$ developing retina leads to alterations in cell fate, particularly toward photoreceptor production. To test this prediction, we stained VSX2-SE adult retinae with different cell-type markers and quantified the number of each cell type in comparison with wild-type retinae. Indeed, results indicated a significant increase in the proportions of photoreceptors (rods and cones) as well as Müller glia in the VSX2-SE-deficient retina compared with the wild-type retina (Fig. 4B). At the molecular level, we performed western blot analyses for CRX, a transcription factor expressed in photoreceptors, in the adult VSX2-SE$^{-/-}$ retinae and detected a significant increase in its protein levels when compared with heterozygous and wild-type littermates (Fig. S4B). Thus, although the VSX2-SE element is dispensable for retinal proliferation, it is required for proper cell fate specification and differentiation.

We next analyzed cell fate in adult VSX2-EN1-deficient retinae. Whereas the retina is microphthalmic and the optic nerve is underdeveloped (Fig. S4C), immunostaining with cell-type markers indicated that all major retinal cell types were born, including bipolar cells (Fig. 4A). We confirmed the presence of bipolar cells by immunostaining the retina with several bipolar cell markers (PKCa, OTX2 and VSX2), albeit their numbers are significantly reduced (Fig. 4C,D). Overall, our functional analysis of the *Vsx2* enhancer landscape revealed distinctive roles for *Vsx2* enhancer components in promoting proliferation and cell fate specification during retinal development.

Structural and functional defects in VSX2-SE$^{-/-}$ retina

The absence of retinal bipolar cells from retinae lacking *Vsx2* enhancer elements motivated us to quantitatively assess defects in retinal thickness. We performed optical coherence tomography (OCT) imaging on live adult VSX2-SE$^{-/-}$ mice and their age-matched heterozygous and wild-type littermates. We found that, overall, the retina was about 20% thinner in VSX2-SE$^{-/-}$ animals, which is attributed to the significant decrease in the INL and inner plexiform layer (IPL) thickness (Fig. 5A-D). The ONL was slightly but significantly thicker, in agreement with the increase in photoreceptor production in retinae lacking the VSX2-SE element (Fig. 5E).

Visual acuity tests of VSX2-SE$^{-/-}$ mice indicated that they are blind (Norrie et al., 2019); however, how the physiological functions of the retina were impaired by the loss of the *Vsx2* super-enhancer remains unclear. To assess this, we performed electroretinography (ERG) examinations on adult VSX2-SE$^{-/-}$ animals and their age-matched heterozygous and wild-type littermates, and found that the b-wave (produced mainly by retinal bipolar cells) was completely absent in the VSX2-SE$^{-/-}$ mice, whereas the a-wave signal (generated by photoreceptors in response to light) remained intact (Fig. 5F-I). In fact, at an elevated light intensity, the response of photoreceptors became slightly stronger in VSX2-SE$^{-/-}$ animals (Fig. 5G). These data indicate that photoreceptor cells are functional in the VSX2-SE$^{-/-}$ retinae, whereas the absence of bipolar cells prevents the propagation of neuronal signals generated by photoreceptors to other retinal neurons.

VSX2 occupies a *Prdm1 cis*-regulatory element and can suppress its activation

To further delineate potential molecular mechanisms underlying the overproduction of rod photoreceptors observed in the VSX2-SE$^{-/-}$ retina, we focused our attention on early events of rod versus bipolar cell fate choice. Previous data suggested that retinal bipolar cells and rod photoreceptors share common precursors: the OTX2-expressing cells (Brzezinski and Reh, 2015; Fossat et al., 2007). In a subset of OTX2-positive precursor cells in the postnatal retina, OTX2 positively regulates the expression of either Vsx2 or Prdm1, promoting bipolar or rod cell fate, respectively (Katoh et al., 2010; Wang et al., 2014; West and Cepko, 2022). Within this context, overexpression of Prdm1 promotes rod formation by inhibiting *Vsx2* expression (Brzezinski et al., 2010; Goodson et al., 2020a). Whether VSX2 represses *Prdm1* expression remains unclear (Goodson et al., 2020a; West and Cepko, 2022). In WT developing retina, *Prdm1* expression peaks at P4 and is downregulated thereafter (Fig. 6A; Brzezinski et al., 2010).

Development (2022) 149, dev200642. doi:10.1242/dev.200642

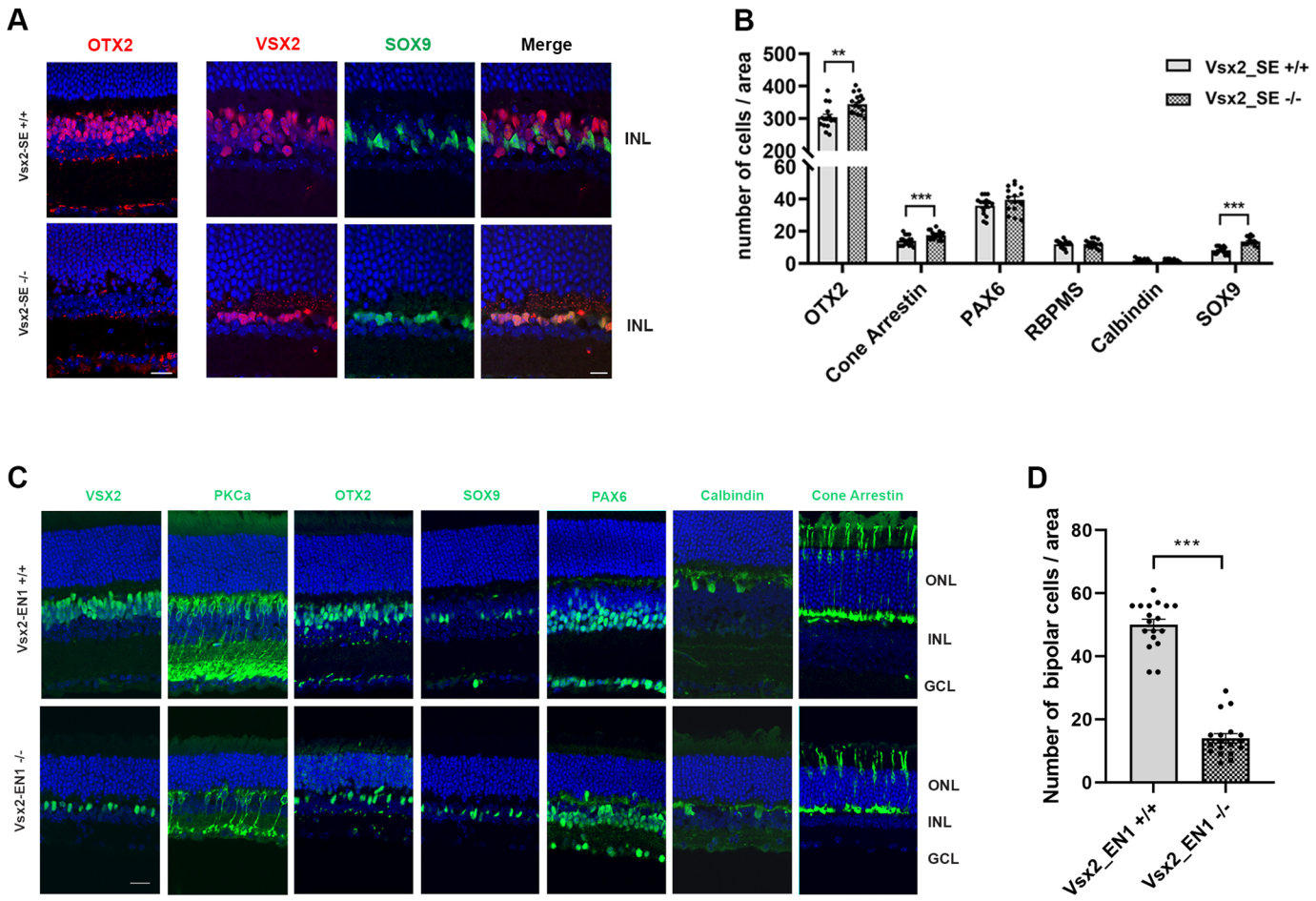

Fig. 4. Analyses of cell fate acquisition in *Vsx2* enhancer-deficient retinas. (A) Adult retina immunoassayed with OTX2 antibody revealing a complete loss of bipolar cells in VSX2-SE knockout retina. Scale bar: 20 µm. Co-immunostaining of VSX2 and the Müller glia marker SOX9 in wild-type and VSX2-SE knockout mice. Scale bar: 10 µm. (B) Quantification of the cell numbers in retinae from VSX2-SE$^{-/-}$ and their wild-type littermates immunostained with different cell type markers (data are mean±s.e.m., n=3 retinae for each mouse line; ***P<0.001; **P<0.01; two-tailed unpaired Student's t-test). (C) Adult retinal cryosections from wild-type and VSX2-EN1-deficient mice immunoassayed with different cell-type-specific markers. VSX2, PKCa and OTX2 (labeling retinal bipolar cells), PAX6 (RGCs and amacrine cells), calbindin (horizontal cells) and cone arrestin (cone photoreceptors). Antibodies used are described in the Materials and Methods. (D) Quantification of bipolar cell numbers in retinae from VSX2-EN1$^{-/-}$ and their wild-type littermates (n=3 retinae for each mouse line; ***P<0.001; two-tailed unpaired Student's t-test). ONL, outer nuclear layer; INL, inner nuclear layer; GCL, ganglion cell layer.

Consistent with the overproduction of photoreceptors in the VSX2-SE$^{-/-}$ adult retinae, we detected an increase in PRDM1 levels as early as P10 (Fig. 6A-C).

To explore this observation on a deeper level, we reasoned that VSX2 might directly bind and repress *Prdm1* regulatory elements. We first profiled the *Prdm1* enhancer landscape during retinogenesis using our previously published ATAC-Seq data (Aldiri et al., 2017) and found several peaks correlating with its expression (Fig. 6D). ChIP-Seq analysis of VSX2 in the adult murine retinae revealed that VSX2 occupies regulatory elements near to *Prdm1*, including an enhancer region that is necessary and sufficient for the retinal expression of *Prdm1* (Fig. 6D) (Mills et al., 2017; Wang et al., 2014). VSX2 occupancy on this *Prdm1* regulatory element is observed in the adult retina, when *Prdm1* expression has subsided, but not in the E14.5 retina, when the expression is active (Fig. 6D; (Brzezinski et al., 2010)).

We then tested whether VSX2 can directly suppress *Prdm1* enhancer activities using luciferase assays (Fig. 6E). Although data hinted at a repressive activity by VSX2, it was not statistically significant (Fig. 6E). Earlier studies have shown that OTX2 is required for *Prdm1* expression, an effect mediated by OTX2 binding to *Prdm1* enhancer elements (Mills et al., 2017; Wang et al., 2014). By investigating ChIP-Seq data of OTX2 (Samuel et al., 2014) and VSX2 (this article) we found that OTX2 and VSX2 co-occupy the *Prdm1* regulatory region that is important for its expression in mouse and human adult retinae (Fig. 6D). Transfection of Otx2 led to a significant increase in *Prdm1* enhancer activities in luciferase assays, consistent with its role in activating *Prdm1* expression (Fig. 6E) (Wang et al., 2014). However, co-transfection of Vsx2 and Otx2 led to a significant decrease in the ability of OTX2 to activate the *Prdm1* enhancer, suggesting that VSX2 can repress OTX2-mediated activation of *Prdm1* (Fig. 6E). Finally, we tested whether OTX2 and VSX2 physically interact. Co-IP experiments performed at P7 and in the adult mouse retina confirmed this hypothesis (Fig. 6F). Taken together, these data underscore the involvement of VSX2 in positive and negative transcriptional regulatory loops, whereby VSX2 governs the activities of its enhancer, as well as regulatory elements of genes driving proliferation and cell-type acquisitions, in association with known transcription factors important for retinal development.

Development (2022) 149, dev200642. doi:10.1242/dev.200642

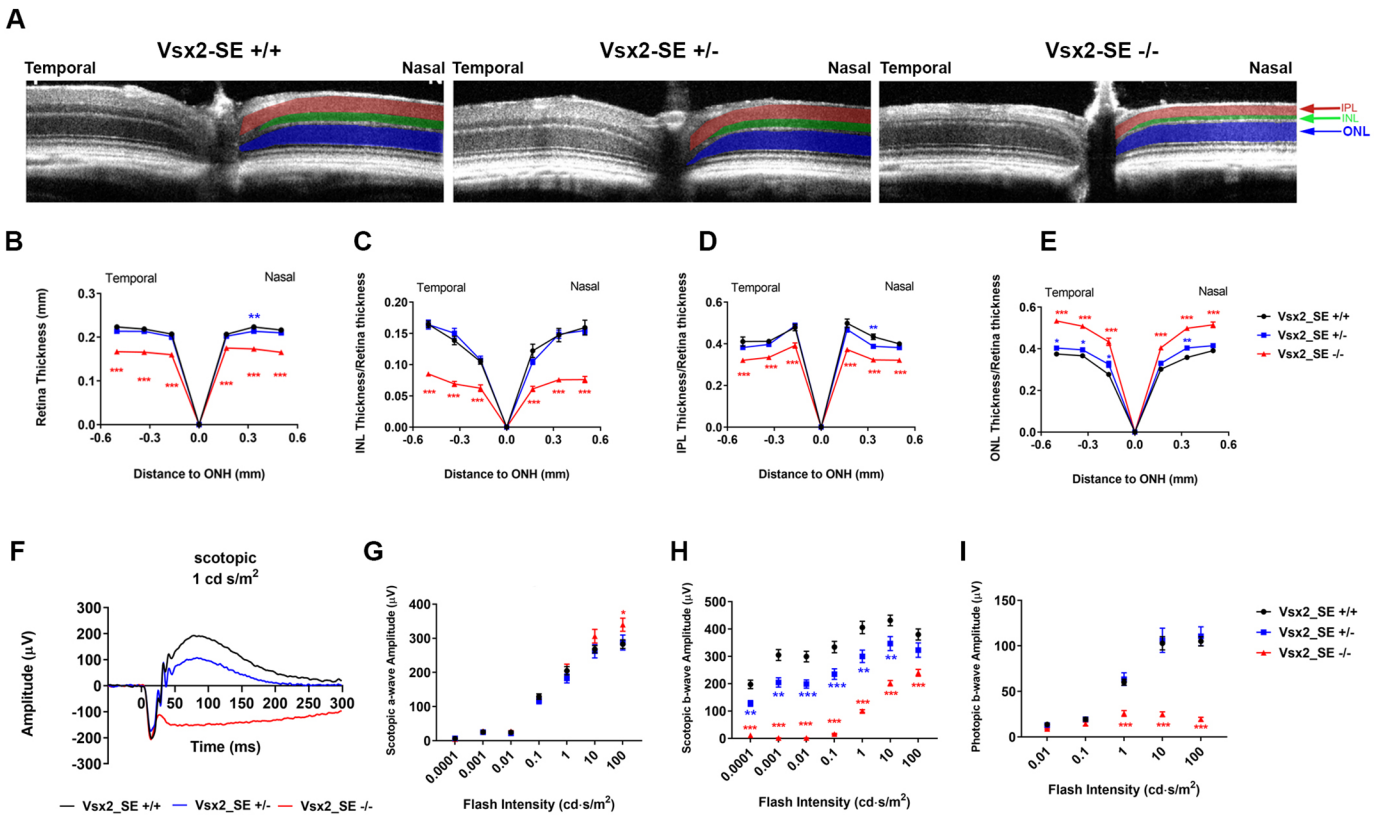

Fig. 5. Structural and functional defects in VSX2-SE$^{-/-}$ retina. (A-I) Abnormal retinal structure and function in VSX2-SE-deficient retina. (A) OCT scans of age-matched adult VSX2-SE$^{-/-}$ animals and littermate heterozygous and wild-type controls. The IPL, INL and ONL were pseudo-colored at the nasal side for easier recognition. (B-E) Quantification of retinal layer thickness from wild-type, heterozygous and homozygous VSX2-SE littermate mice (n=5 for each group). (F) Representative electroretinograms (ERGs) of age-matched adult *Vsx2*-SE$^{-/-}$, heterozygous and wild-type littermates measured at 1 cd s/m^2. The b-wave is completely absent in the mutant retina. (G,H) Scotopic ERG quantifications of a-wave (G) and b-wave (H) amplitudes. (I) Photopic ERG quantifications of the b-wave (n=5 for each group). Data are mean±s.e.m. Two-tailed unpaired Student's t-test was used to compare the differences between heterozygous or homozygous with wild type (n=5; *P<0.05; **P<0.01 ***P<0.001).

Evolution-based functional dissection of the *Vsx2* enhancer during retinogenesis

Recent data indicate that conserved enhancer elements that regulate genes crucial for animal survival and function are usually under evolutionary constraints to limit non-coding mutations that are detrimental to the expression of their respective genes (Zhen and Andolfatto, 2012). A recent study on subterranean moles, in which vision is largely non-essential, found a statistically significant (accelerated) mutation rate in non-coding sequences near to genes essential for vision, thus providing an indirect assay to measure the functionality of non-coding regulatory DNA associated with retinal genes based on sequence divergence (Partha et al., 2017). With this in mind, we used this evolutionary approach to further understand the functional importance of the VSX2-bound regions in the *Vsx2* enhancer landscape. We scanned the mole acceleration profile (Partha et al., 2017) in the *Vsx2* genomic landscape and discovered several significantly divergent sequences, most of which lie within the *Vsx2* super-enhancer, suggesting that evolutionary constraints that safeguard *Vsx2* enhancer sequences have been relaxed in subterranean moles (Fig. 7A). The only exception was the EN2 region, where no evidence for sequence deterioration was observed (Fig. 7A).

By examining the mole acceleration data, we also noticed the presence of a *Vsx2* intronic domain that remained highly conserved and occupied by CTCF, a highly conserved transcription factor with ubiquitous expression and diverse roles in eukaryotes (Fig. 7A; blue bar) (Kim et al., 2015). Importantly, CTCF regulates the 3D chromatin architecture, in part by establishing enhancer-promoter contacts, suggesting a possible regulatory role within the *Vsx2* enhancer landscape (Daghsni and Aldiri, 2021; Merkenschlager and Nora, 2016). To test the functional significance of this CTCF-bound region, we deleted this CTCF-binding site using CRISPR/Cas9 technology (Fig. S4C), and analyzed *Vsx2* expression and retinal structure and function in two independent mouse sublines that carry the deletion. Our data indicated that this CTCF-bound site was completely dispensable for *Vsx2* expression and overall retinal development, as no evidence for a change in *Vsx2* expression levels, bipolar cell genesis or retinal morphology was found (Fig. S4D-F). Furthermore, ERG analysis indicated that the *Vsx2*-CTCF$^{-/-}$ retina remained fully functional (Fig. S4G,H). Thus, although this CTCF-bound region is highly conserved, its functional significance remains unknown.

To further test whether the *Vsx2* enhancer autoregulatory module is conserved in humans, we performed ChIP-Seq for VSX2 on adult human retinae, identifying 14,000 peaks (Fig. 7B-D; Table S5). Motif analysis of sequences in peak summits was consistent with the mouse data in which Q50 homeodomain-containing transcription factors were over-represented (Fig. 7C). The VSX2 genome-wide profile in the human retina also revealed extensive binding of photoreceptor and bipolar genes [58.3% (81/139) for rods, 137/255 (53.7%) cones and 48/102 (47.1%) for bipolar gene signatures], in agreement with mouse VSX2 ChIP-Seq data (Table S5). Examples

Development (2022) 149, dev200642. doi:10.1242/dev.200642

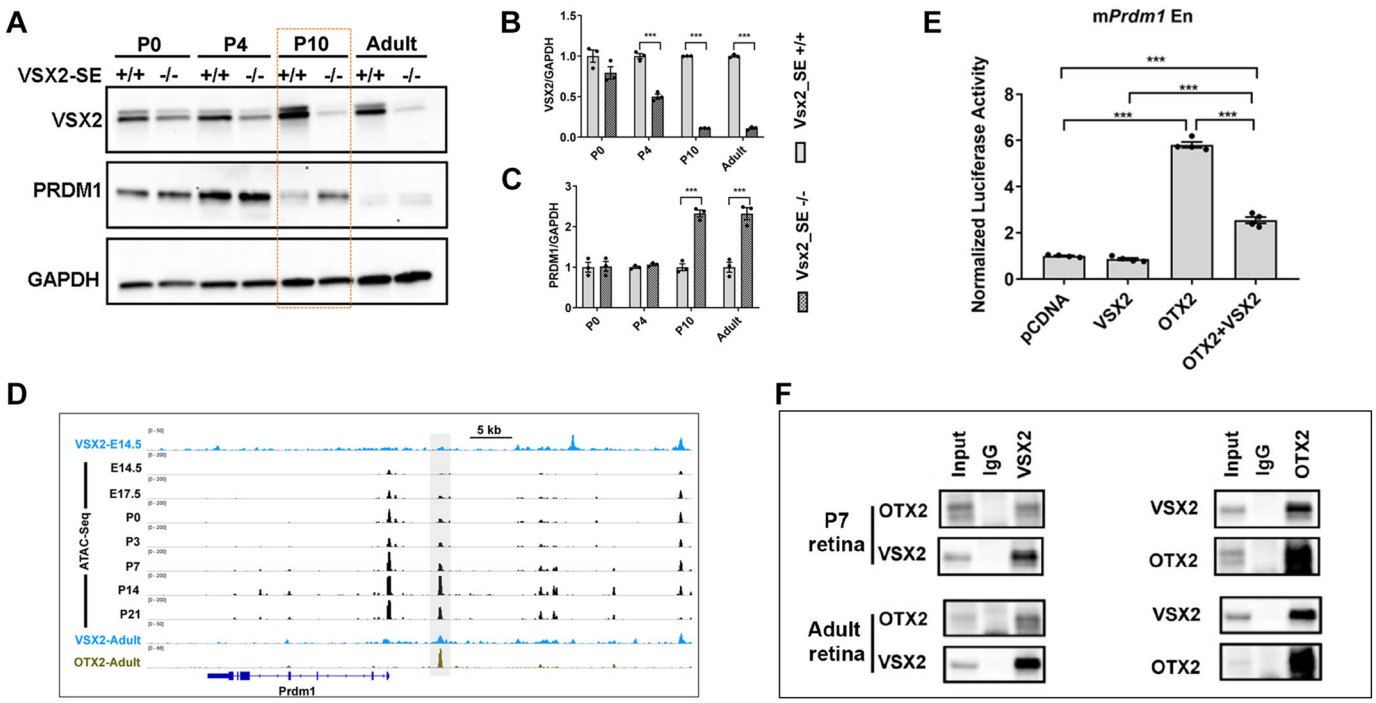

Fig. 6. Regulation of the Prdm1 enhancer by VSX2. (A-C) Western blot analysis of VSX2 and PRDM1 protein levels in P0, P4, P10 and adult retinae (A) with quantifications shown in B and C (n=3 for each stage). Rectangular outline in A indicate the stage with a pronounced increase in PRDM1 expression. Data are mean±s.e.m., n=3; ***P<0.001; **P<0.01; *P<0.05; two-tailed unpaired Student's t-test). (D) Chromatin profile of *Prdm1* genomic landscape during mouse retinal development, as revealed by ATAC-Seq (data from Aldiri, et al., 2017), VSX2 ChIP-Seq (in E14.5 and adult retinae) and OTX2 ChIP-Seq from the adult retina (Samuel et al., 2014). The highlighted region indicates the position of an OTX2/VSX2-bound regulatory element (in the adult mouse retina) that was used in the luciferase assay. This enhancer region contains elements shown to be necessary and sufficient for *Prdm1* expression. (E) Luciferase assay of mouse *Prdm1* enhancer activities in the presence of Vsx2 and/or Otx2. 293T cells were co-transfected with vectors expressing Vsx2 or/and Otx2 along with a reporter plasmid containing *Prdm1* enhancer (data are mean±s.e.m., n=4; ***P<0.001; two-tailed unpaired Student's t-test). (F) Co-IP assay performed on cell lysates of P7 mouse retina (upper panel) and adult mouse retina (lower panel) showing interaction of VSX2 and OTX2. Antibodies used for immunoprecipitation and western blot are indicated above and on the left of the panels. 5% input was used.

of genes bound by VSX2 are *NEUROD4* (bipolar), *CRX* (photoreceptors), *THRB* (cones) and *PRDM1* (rod precursors) Fig. 7D). Importantly, VSX2 ChIP-Seq in the human retina indicated that the VSX2-binding profile near to the VSX2 locus is conserved (Fig. 7D), with VSX2 peaks (except EN2) exhibiting significant deterioration in mole (Fig. 7A).

DISCUSSION

Transcriptional enhancers function as platforms for recruiting transcription factors to mediate spatial and temporal regulation of gene expression (Buecker and Wysocka, 2012). *Vsx2* plays a crucial role during retinogenesis, controlling multiple levels of retinal proliferation and differentiation, but much remains unknown about how it exerts its function and influences the retinal genome. Our genome-wide profiling of VSX2 occupancy during retinal development provides insight into the gene networks regulated by VSX2, and functional investigations of its regulatory elements reveal distinct regulatory modules that operate at the chromatin level. One of these loops involves a synergistic association with PAX6 in the proliferative retina to positively regulate *Vsx2* expression itself. The key importance of this coordination is evidenced by genetic studies in humans and mice, illuminating analogous proliferation defects associated with VSX2 and PAX6 gene-coding mutations (Ferda Percin et al., 2000; Slavotinek, 2011).

Whereas our data point towards the involvement of an autoregulatory module in the maintenance and/or amplification of *Vsx2* expression, the mechanisms by which *Vsx2* expression is initiated in the developing retina remain unclear. Additionally, our luciferase assays indicate that the Vsx2 R200Q mutation, although showing a significant reduction in its ability to transactivate *Vsx2* enhancers, retains significant residual activity when combined with Pax6 (Fig. 2B). This is consistent with *in vivo* evidence demonstrating that mouse lines bearing the R200Q mutation still express *Vsx2* and underscores the complexity of *Vsx2* regulation during retinogenesis (Zou and Levine, 2012).

We speculate that the coordination between VSX2 and PAX6 in RPCs is not limited to *Vsx2* regulatory elements, that it may involve other transcription factors and chromatin regulating proteins, and that this coordination is likely to exist in a group of proliferation-associated genes. Furthermore, the interaction between PAX6 and VSX2 is limited to RPCs, given that the expression of *Pax6* and *Vsx2* becomes mutually exclusive in the adult retina.

One of the noteworthy features of the *Vsx2* enhancer is that it remains active and is extensively bound by VSX2 in retinal bipolar cells; current evidence implicates OTX2 in regulating *Vsx2* expression in the postmitotic retina (Goodson et al., 2020a; Kim et al., 2008; West and Cepko, 2022). Indeed, our co-IP results revealed a robust physical interaction in the adult retina. Thus, it will be interesting to functionally examine whether VSX2 and OTX2 act to regulate elements of the *Vsx2* enhancer landscape and other factors required for retinal bipolar differentiation.

Vsx2 expression in Müller glia in the VSX2-SE$^{-/-}$ retina has not been lost, mirroring its status in RPCs and underscoring shared properties between RPCs and Müller glia (Jadhav et al., 2009). We

Development (2022) 149, dev200642. doi:10.1242/dev.200642

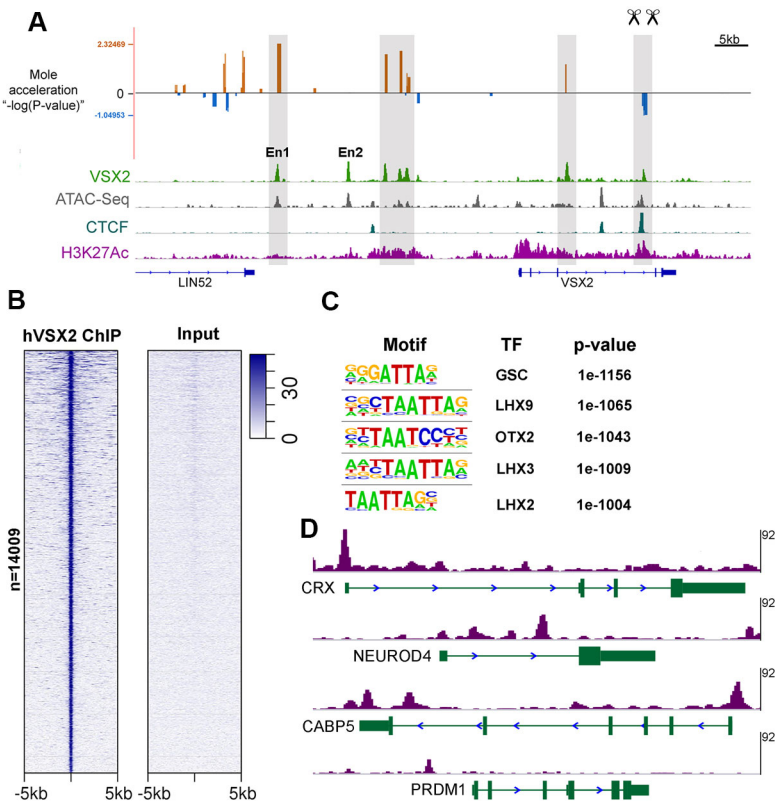

Fig. 7. Evolution-based analysis of *Vsx2* enhancer landscape. (A) Mole acceleration track near VSX2 overlaid on the chromatin signature of the adult human retina. ATAC-Seq, CTCF and H3K27Ac ChIP-Seq sequencing data were obtained from Cherry et al. (2020). Shaded areas represent regulatory regions occupied by VSX2 with significant sequence deterioration (orange bars) or conservation (blue bars). The EN2 sequence is not significantly deteriorated. (B-D) VSX2 ChIP-Seq analysis on the human adult retina. (B) Heatmap of ChIP-Seq binding signal intensity for VSX2 and input. (C) Top five enriched motifs in VSX2-binding regions in the adult human retina, as analyzed by HOMER. (D) Genome browser snapshots of VSX2 peaks near to CRX (photoreceptors), NEUROD4 and CABP5 (bipolar cells), and PRDM1 (rod precursors). VSX2 binding to the PRDM1 enhancer is conserved.

propose a model in which the *Vsx2* regulatory landscape contains elements that function in a complementary non-redundant manner to promote robust *Vsx2* expression and ensure proper progression of retinal proliferation and differentiation. Interestingly, preliminary evidence suggests that *Vsx2* expression in the developing ventral spinal cord is maintained in our *Vsx2* enhancer knockouts, adding a layer of complexity to the regulation of *Vsx2* during neurogenesis (Fig. S4I-K). It is likely that *Vsx2* expression in RPCs, Müller glia and bipolar cells can be temporally and spatially uncoupled, thus allowing us to predict the presence of additional regulatory elements that are essential for *Vsx2* expression.

As this article was in preparation, a report described several deletions in the mouse *Vsx2* non-coding regulatory elements, including VSX2-EN1 region (Honnell et al., 2022). Overall, the analysis reported by Honnell et al. is consistent with ours, showing a strong effect on retinal proliferation upon loss of VSX2-EN1 element. Interestingly, although a deletion in VSX2-EN2 seems to have a mild phenotype in retinal development, targeting both EN1 and EN2 leads to microphthalmia, with eye size smaller than that observed after single deletions, suggesting an additive effect of both enhancer constituents (Honnell et al., 2022). Honnell and co-authors also confirmed previous work demonstrating the presence of a regulatory element 17 kb from *Vsx2* that is required for the bipolar cell genesis (Goodson et al., 2020a); our ChIP-Seq data indicate that this region is occupied by VSX2 in mouse and human retina (Figs 2A and 7A). Taking all these studies into account, we conclude that the *Vsx2* enhancer landscape contains elements that function prominently during specific developmental windows to control aspects of retinal proliferation and bipolar cell differentiation.

The VSX2 binding of non-bipolar cell signature genes is in agreement with the hypothesis that VSX2 maintains retinal bipolar cell identity by suppressing inappropriate temporal and spatial transcriptional programs, particularly those related to rod photoreceptors (Clark et al., 2008; Dorval et al., 2006; Livne-Bar et al., 2006; Murphy et al., 2019). Our motif analysis of VSX2 peaks indicates a significant enrichment of Q50 motifs, which are favorably recognized by homeodomain transcription factors with known repressive and activating functions, including VSX2 (Clark et al., 2008; Green et al., 2003; Hughes et al., 2018; Murphy et al., 2019). The current model suggests that Q50 sequences bound by VSX2 are predominantly associated with repressive functions, primarily targeting rod genes (Murphy et al., 2019). Thus, it is likely that the analysis reflects the widespread occupancy of VSX2 on photoreceptor-related regulatory elements in bipolar cells. The transcriptional regulation by Q50 proteins can be altered by binding co-factors (Slattery et al., 2011). As such, VSX2 can promote the expression of bipolar genes and the suppression of rod photoreceptors in bipolar cells based on selective recruitments of co-activators or co-repressors.

Notably, *Prdm1* is a target of VSX2 in mouse and human adult retina, and its enhancer activities mediated by OTX2 can be suppressed by VSX2 *in vitro*. Our data complement a proposed gene regulatory network that involves VSX2, OTX2 and PRDM1, whereby VSX2 is suggested to suppress rod differentiation by inhibiting *Prdm1* expression during the bipolar cell specification (Goodson et al., 2020a; Wang et al., 2014; West and Cepko, 2022). Consistent with this model, studies indicate that VSX2 can function as a transcriptional repressor and earlier work has demonstrated that loss of *Vsx2* in the postmitotic retina leads to an increase in photoreceptor cells (Goodson et al., 2020a; Livne-Bar et al., 2006). Although our data further support this modulatory regulatory network, more work is required to explore whether VSX2 directly suppresses *Prdm1* expression in bipolar cell precursors *in vivo*.

Our evolutionary analysis involving mole acceleration data of the *Vsx2* regulatory landscape provides support to our functional

Development (2022) 149, dev200642. doi:10.1242/dev.200642

interrogation. Murine *Vsx2* enhancer deletions generated by our group and others indicate that non-regulatory elements with a significant mutation rate in the mole are functionally important for retinal development (Fig. 7A) (Goodson et al., 2020a; Honnell et al., 2022; Norrie et al., 2019). No significant changes in mutation rate were detected in the EN2 region, which is in agreement with results from the knockout mice showing only a mild effect on retinal development upon loss of EN2 element (Honnell et al., 2022). On the other hand, removing a highly conserved CTCF binding site in the *Vsx2* intronic region had no obvious effect on retinal development, implying that this site is not involved in *Vsx2* promoter-enhancer contacts or that those contacts are dispensable for *Vsx2* expression. The mole acceleration data predict the presence of additional sites that might be functionally relevant (Fig. 7A), but whether these sites are biologically important remains to be tested. Overall, our analysis provides the basis for an in-depth understanding of the gene regulatory network controlled by VSX2, revealing the diverse roles it plays during retinogenesis, and underscoring how the chromatin landscape influences essential aspects of retinal cell fate determination.

MATERIALS AND METHODS

Animals

All mice were maintained in accordance with the guidelines set forth by the Institutional Animal Care and Use Committee of the University of Pittsburgh. C57 BL/6J animals were purchased from Jackson Laboratory.

Mouse enhancer knockouts

B6D2 (C57 BL/6J×DBA/2J F1) females (6-8 weeks old) were stimulated by administration of 5 IU of PMSG through intraperitoneal injection at 3:30 pm on day 1, 5 IU of hCG 48 h after PMSG injection, then mated to B6D2 F1 stud males. Embryos were collected from oviducts the following morning and were cultured in KSOM medium in 5% CO_2 at 37°C until electroporation. Embryos were electroporated with 100 ng of Cas9 protein and 200 ng/µl of gRNAs each in an Opti-MEM medium. gRNAs were tested prior to embryo injection for activity in mouse N2A cells using targeted next-generation sequencing as previously described (Sentmanat et al., 2018). Electroporation was performed using the Super electroporator NEPA21 type II and CUY 501-1-1.5 electrode (NEPA GENE) under the following conditions: poring pulse (voltage 40 V, pulse length 2.5 ms, pulse interval 50 ms, number of pulses 4, decay rate 10%, polarity +); and transfer pulse (voltage 7 V, pulse length 50 ms, pulse interval 50 ms, number of pulses 5, decay rate 40%, polarity +/=). After electroporation, the embryos were washed twice in KSOM medium, then cultured in KSOM medium overnight in 5% CO_2 at 37°C. On the following day, the two-cell stage embryos were transferred to the oviducts of pseudopregnant CD1 females (0.5 dpc). The resulting founder animals (P0) were genotyped using PCR and Illumina Mi-Seq to identify mice with desired deletions. Adult animals positive for deletion were backcrossed to C57 BL/6J to generate wild-type, heterozygous and homozygous animals. Mouse genotyping was determined by PCR and then confirmed with Sanger sequencing. The following guides were used to generate the knockout lines: VSX2-SE-KO 5′ guide, 5′-GCAGGCCATGTGCTCGTCGANGG-3′; VSX2-SE-KO 3′ guide, 5′-CAGGGTGCAGGCTGACAACGNGG-3′; VSX2-EN1-KO 5′ guide, 5′-GTTAGACCTAGTCAGAACTCNGG-3′; VSX2-EN1-KO 3′ guide, 5′-TACTTCAGACTCTGGCTCCANGG-3′; VSX2-CTCF-KO 5′ guide, 5′-GAGTCTCTAAAAGTAGGAAANGG-3′; VSX2-CTCF-KO 3′ guide, 5′-ACCTAATCAAGCAATCAAGTNGG-3′. Details of the VSX2, VSX2-EN1 and VSX2-CTCF primers are provided in Table S6.

Zebrafish reporter assay

Tol2 Transposase mRNA

pCS2FA-transposase was used for *in vitro* transcription of capped Tol2 transposase mRNA. Selected enhancers were PCR amplified and cloned in the pDestTol2pA2 vector, upstream of the eGFP. pCS2FA plasmid DNA was digested with Not1 and purified with Qiagen kit. Linearized DNA was used as a template for *in vitro* transcription using a mMACHINE SP6 Transcription Kit. Purified mRNA was adjusted to a concentration of 250 ng/µl and aliquoted for microinjection. The following primers were used in cloning *Vsx2* mouse and human enhancer fragments (restriction enzyme sites are underlined): mVsx2_En1_BamHI forward, TAAAGGATCCCCTTCCCACCTTTTGTCTGGTA; mVsx2_En1_-BamHI reverse, GAAAGGATCCTGTGCTCGTCGAGGGTAGACT; mVsx2_En2_BamHI forward, TAAAGGATCCCCCGGGCTTAGAGA GCATTT; mVsx2_En2_BamHI reverse, GAAAGGATCCCAGGCAC-TTCCCAAGGAGAG; hVsx2_En1_BamHI forward, TAAAGGATCCT-TGTCTATGCCTAAAGAGGCCA; hVsx2_En1_BamHI reverse, GAAA-GGATCCTTCTAGGGCAGAATTCACTCACG; hVsx2_En2_HindIII forward, TAAAAAGCTTGAGAAGCCTGAGGTTTAGCGATT; hVsx2-_En2_HindIII reverse, GAAAAAGCTTCTCCACAAGCATGATCCT-ACTGA.

Microinjection

Constructs containing mouse and human VSX2-EN1 and VSX2-EN2 were injected along with transposase mRNA into one-cell stage AB wild-type zebrafish embryos. The injection volume was calibrated to 1 nl. 25 pg and 50 pg of transposase mRNA were injected per construct. Injected embryos were transferred to a petri dish and incubated at 28.5°C. After 24 h, the embryos were examined for EGFP expression under a fluorescent dissecting microscope (Axio Zoom V.16) to determine the stereotypic expression pattern conferred by the enhancer. The total number of embryos injected with the construct and the number of embryos with the stereotypical EGFP pattern were determined to calculate the frequency of the pattern. Injection experiments were repeated three times, into embryos derived from different AB parents, for biological replicates.

Imaging and sectioning

Embryos were dechorionated and imaged using a Leica M165FC stereoscope digital camera. Sectioning was carried out according to the protocol of Uribe and Gross (2007). Briefly, embryos were fixed in 4% paraformaldehyde in PBS (pH 7.4) for 24 h at 4°C. After fixation, the eyes were sucrose-protected and embedded in tissue-freezing medium (TBS, Waltham, MA, USA). The eyes were sectioned at 12 µm on a Leica CM1850 cryostat and the sections were collected on Superfrost/Plus slides (Thermo Fisher Scientific), dried and stored at−20°C.

Luciferase reporter assay

cDNA of human and mouse Vsx2 and Pax6 were subcloned into pcDNA3, with CMV promoter replaced by EF1α. Mouse and human enhancer fragments were cloned in Nanluc plasmid containing minimal promoter pNL3.1[Nluc/minP] (Promega N1031) using standard cloning techniques. Deletion of VSX2 predicted binding sites was achieved by overlap extension PCR, which has been described before (Lee et al., 2004). Primer sequences are provided in Table S7.

HEK293T cells (ATCC CRL-3216) were cultured in DMEM (Thermo Fisher Scientific, 10569044)+10% FBS (Thermo Fisher Scientific, 16000036)+100 U/ml penicillin, 100 µg/ml streptomycin (Thermo Fisher Scientific, 10378016). Cells were plated in 24-well plates seeded at 30,000 cells per well and allowed to adhere overnight. For Vsx2 enhancer elements, 500 ng of Vsx2 and/or Pax6 constructs were co-transfected with 200 ng of Vsx2 enhancer vectors. For the Prdm1 enhancer, 100 ng of Otx2 and/or Vsx2 vectors were transfected with 200 ng of Prdm1 enhancer. In all cases, 10 ng of firefly luciferase plasmid (pGL4.53[luc2/PGK]; Promega E5011) were delivered.

Transfection was performed using Lipofectamine 3000 (Thermo Fisher Scientific, L3000008) in each well. Empty vectors co-transfected with each of the enhancer constructs and firefly luciferase plasmid (pGL4.53[luc2/PGK]) were used as a control. Cells were lysed and assayed 24 h after transfection using Nano-Glo Dual-Luciferase Reporter (NanoDLR) assay system (Promega N1610) according to the manufacturer's protocol. Luminescence measurements were taken as singlets using a SpectraMax M5 (Molecular Devices) plate reader. Experiments were performed in quadruplicate.

Development (2022) 149, dev200642. doi:10.1242/dev.200642

Western blot

Retina samples were lysed in 100 µl RIPA buffer [1% Triton X-100, 0.5% sodium deoxycholate, 0.1% SDS, 0.15 M NaCl, 50 mM Tris (pH 7.5), 1 mM EDTA] and protease inhibitor cocktail (Complete Mini-EDTA free, 11836170001, Roche). One retina from adult mouse or two or three retinas from pups were pooled for each lysate preparation. Protein concentrations were determined by BCA kit (23225, Thermo Fisher Scientific). 20 µg of total protein was loaded per well onto an SDS-PAGE gel and transferred to PVDF membrane. After blocking with 5% nonfat dried milk in TBS-Tween, the membranes were incubated with the appropriate primary antibodies. Immunoblots were quantified by the ImageJ program.

Immunoprecipitation

HEK-293T cells were transfected with DNA constructs using Lipofectamine 3000 (Invitrogen) in a six-well plate. Two days after transfection, cells were lysed with high-salt lysis buffer [10% glycerol, 50 mM Tris (pH 7.5), 300 mM NaCl+1% NP-40, 2 mM $MgCl_2$] with a protease inhibitor cocktail and rotated for 30 min at 4°C. An equal volume of no-salt lysis buffer [10% glycerol, 50 mM Tris (pH 7.5), 1% NP-40+2 mM $MgCl_2$] was added to cell lysates to reduce salt concentration. 500 µg of protein was incubated with the appropriate antibodies overnight. For endogenous immunoprecipitation, non-denatured native protein lysates from C57 BL/6J E14.5 or adult retinae were prepared using COIP buffer (PBS+10% glycerol +0.6% Triton x-100) with protease inhibitors. On average, 30 retinae from E14.5 or five retinae from adult mice were pooled for each lysate preparation. Equivalent volumes of cell lysates were incubated with the appropriate antibodies or IgG overnight. The next day, protein A/G magnetic beads (88802, Thermo Fisher Scientific) were added and incubated for 3 h, washed with low-salt lysis buffer [10% Glycerol, 50 mM Tris (pH 7.5), 150 mM NaCl+1% NP-40, 2 mM $MgCl_2$) five times. Beads were eluted with SDS/PAGE loading buffer and subjected to SDS/PAGE and western blotting. Different species of secondary antibodies were used for detection to avoid heavy chain contamination (~50 kDa). Antibodies used in western blots and immunoprecipitation are listed in Table S8.

Electroretinogram

Electroretinograms (ERGs) were performed using the Celeris system (Diagnosys), as described by Liu et al. (2020). Before each test, 6-week-old mice were dark-adapted overnight. Mice were anesthetized by an intraperitoneal injection of ketamine/xylazine (80 mg/kg bw/7 mg/kg bw), and eyes were then treated with 1% tropicamide (Akorn) and 2.5% phenylephrine hydrochloride. Eyes were lubricated using a 0.3% hypromellose eye gel (Alcon) before the electrodes are applied. Scotopic ERG responses of dark-adapted eyes to seven flashes from 0.0001 cd·s/m^2 to 100 cd·s/m^2 were recorded and averaged from ten sweeps per flash intensity with inter-sweep intervals of 10 to 30 s. After exposure to 10 cd/m^2 illumination for 10 min, the photopic ERG responses were recorded from the light-adapted eyes in response to flashes from 0.01 cd·s/m^2 to 100 cd·s/m^2 in addition to a 10 cd/m^2 background light. Each group contained five mice. A-wave and B-wave amplitudes of each ERG recording were measured and averaged from five animals.

Optical coherence tomography (OCT) imaging

Noninvasive ultra-high-resolution spectral domain optical coherence tomography (SD-OCT) (Bioptigen) was performed for *in vivo* imaging of mouse retinae (Chen et al., 2018). Briefly, mice at 6 weeks of age were anesthetized using an intraperitoneal injection of ketamine/xylazine (80 mg/kg bw/7 mg/kg bw). Pupils were dilated with 1% tropicamide (Akorn) and 2.5% phenylephrine hydrochloride prior to SD-OCT imaging. Five frames of OCT images were acquired in the B-scan mode, and averaged for image presentation and analysis. The thickness of the INL, IPL, ONL and whole retina was measured along with the scanned SD-OCT image at six points from the nasal to temporal of the retina. Each group had five mice, and graphs of INL, IPL, ONL and whole retina thicknesses were plotted to obtain the mean±s.e.m. of the five animals.

Immunostaining

Eyes were isolated and fixed in 4% PFA overnight at 4°C. After dissection, retinae were equilibrated in 5%, 10%, 20% and 40% sucrose in PBS, and then embedded in a mixture of 40% sucrose in PBS and OCT at a 1:1 volume ratio and frozen. Sections were cut at 17 µm. Retinae were washed three times with PBS with 0.1% Triton and incubated in block solution for 1 h at room temperature and then in primary antibody in block solution overnight at 4°C. The sections were washed three times in PBS and then incubated in secondary antibody for 1 h at room temperature. After washing, sections were incubated with 2 µg/ml Hoechst 33342 (Invitrogen H3570) for 10 min, washed with PBS, then mounted in ProLong Glass Antifade (Invitrogen P36980). Images were acquired with an Olympus Fluoview Confocal microscope (v 4.2). Antibodies used and their dilutions are provided in Table S9.

Electroporation and AP staining

The EN1 and EN2 fragments were amplified from the mouse genomic DNA using the following primers (restriction enzyme sites are underlined): mVsx2_En1_Stagia3 forward, GCCCTCGAGCCTTCCCACCTTTTG-TCTGGTA; mVsx2_En1_Stagia3 reverse, GCCGAATTCTGTGCT-CGTCGAGGGTAGACT; mVsx2_En2_Stagia3 forward, GCCGAATTC-CCCGGGCTTAGAGAGCATTT; mVsx2_En2_Stagia3 reverse, GCC-GAATTCCAGGCACTTCCCAAGGAGAG. Then these fragments were cloned into the Stagia3 vector using restriction enzyme-based methods. The CAG-mCherry plasmid and Stagia3 vector were kind gifts from Dr da Silva's lab (University of Pittsburgh, PA, USA). The plasmids used for electroporation were prepared with a final concentration of 700 ng/µl per plasmid. For electroporation, five pulses at 25 V of 950 ms off and50 ms on were applied to the dissected E15 retinas. Retinas were then carefully transferred to the 12 well plates and cultured for 2 days. The electroporated retinas were then washed with PBS and fixed with 4% PFA for 30 min at room temperature. Before proceeding with AP staining, fixed retinas were checked for the presence of mCherry signal (electroporation efficiency control), as fluorescence intensity becomes very weak after AP staining. The retinas were incubated at 65°C for 1.5 h then with AP buffer [100 mM Trizma, 100 mM NaCl, 5 mM $MgCl_2$ (pH 9.5)] for 15 min at room temperature before being changed to developer buffer (one NBT/BCIP tablet dissolved in 10 ml ultrapure distilled H_2O). AP signal was checked after incubation for at least 20 min at room temperature. The reaction was stopped by washing once with PBS and images for stained retinas were taken using Leica M165 Stereo Microscope. The retinal sections were prepared as follows. The electroporated retinas were washed with PBS and fixed with 4% PFA for 20 min at room temperature, cryoprotected in 5%, 10%, 20% and 40% sucrose in PBS, embedded in a mixture of 40% sucrose in PBS and OCT at 1:1 volume ratio then frozen. Sections were cut at 14 µm and AP staining carried out as described above.

EdU incorporation assay

Click-iT EdU Cell Proliferation Kit (Thermo Fisher Scientific, C10337) was used. Timed pregnant mice (E14.5) were intraperitoneally injected with EdU with a dose of 50 mg/kg body weight. Eyes from the embryos were then collected after 1 h of injection and fixed in 4% PFA for 2-3 h at 4°C. EdU staining was performed on cryosectioned retinas following the manufacturer's protocol.

Quantification of cell number

Eyes from 3-month-old littermates were isolated and fixed in 4% PFA overnight at 4°C. Retinal cryosections were prepared as described in the immunostaining protocol and stained with cell-specific markers: OTX2 for rod photoreceptors; cone arrestin for cone photoreceptors; PAX6 for amacrine cells; calbindin for horizontal cells; SOX9 for Müller glia; and RBPMS for retinal ganglion cells. Sections (three nonoverlapping sections per mouse) demarcating the central retina were identified by the presence of the optic nerve head and subsequently used in the counting. Areas 400 µm away from the optic nerve were used for cell number counts. Three mice per genotype were used.

Development (2022) 149, dev200642. doi:10.1242/dev.200642

Statistical analysis

Statistical analyses and the number of samples (n) are described in detail for each figure panel. A two-tailed unpaired Student's t-test was performed using Excel. All reported P-values were considered significant at $P<0.05$. Data are presented as mean±s.e.m.

RNA preparation and bulk RNA-Seq

Freshly dissected E14.5 retinas were placed in TRIReagent (Zymo Research R2050-1-50) and RNA was extracted according to Direct-zol RNA MiniPrep kit protocol (Zymo Research R2050). RNA integrity was determined using 4200 Agilent Tapestation. Five retinas were used for each biological replicate except for VSX2-EN1 mice, where 15 retinas were used (owing to their small size). Stranded total RNA libraries were prepared following the manufacturer's instructions (Illumina TruSeq Stranded RNA; Ribo-Zero) with the following modifications. Total RNA input was depleted for rRNA and fragmented. Random primers initiated first- and second-strand cDNA synthesis. Adenylation of 3′ ends was followed by adapter ligation and library amplification with indexing. The sequencing was run on a high-output 150-cycle flowcell with read length 2×75 using the Sequencing Platform NextSeq500.

Analysis of bulk RNA-Seq

Raw sequencing reads first went through the pipeline of quality control using Trimmomatic. After pre-processing, surviving reads were aligned to mouse reference genome mm10 by STAR aligner and quantified by read count using HTSeq tool.

Differential expression analyses comparing wild-type and knockout samples were performed by R package DESeq2. Significant changes in gene expression were defined by adjusted P-value lower than 0.05 (FDR=5%) and a fold change greater than 1.5. All the bioinformatics and biostatistical analysis were performed by default parameters.

Chromatin immunoprecipitation

Mouse

In brief, retinae dissected from C57/BL6 mice were flash-frozen and stored at −80°C for subsequent treatment. Retinae were thawed on ice and incubated with 1% formaldehyde in PBS at room temperature for 15 min. Fixation was stopped by the addition of 0.125 M glycine (final). Chromatin was isolated by the addition of lysis buffer and was sheared to an average length of 300-500 bp. Sheared chromatin was precleared with protein G agarose beads (Invitrogen). Chromatin immunoprecipitation (ChIP) was performed on 30-40 µg of sheared chromatin using 6 µl of VSX2 antibody (Exalpha, X1180P).

Complexes were washed, eluted from the beads with SDS buffer, and subjected to RNase and proteinase K treatment to collect DNA. Crosslinking was reversed by incubation overnight at 65°C, and DNA was purified by phenol-chloroform extraction and ethanol precipitation. Prior to Illumina library preparation, qPCR was performed to confirm the significant enrichment of target genes. Two ChIP-Seq biological replicas were performed for each stage.

Human

Eye globes procured post-mortem from two de-identified donors (a 46-year female and a 57-year-old male) without previous medical histories of ophthalmological conditions or interventions were used. The human retinae were dissected within less than 6 h of reported death time, cryopreserved and processed for ChIP protocol as described in the mouse section. The donated organs were obtained via the Center for Organ and Recovery & Education (Pittsburgh, PA, USA). The procurement protocol was approved by the University of Pittsburgh Committee for Oversight of Research and Clinical Training involving Decedents (CORID).

ChIP-sequencing

Illumina sequencing libraries were prepared from the ChIP and input DNAs by the standard consecutive enzymatic steps of end-polishing, dA-addition and adaptor ligation. Steps were performed on an automated system (Apollo 342, Wafergen Biosystems/Takara). After a final PCR amplification step, the resulting DNA libraries were quantified and sequenced on Illumina's NextSeq 500 (75 nt reads, single-end).

Analysis of ChIP data

Sequencing reads were aligned to mouse (mm10) or human (hg38) reference genomes by Burrows-Wheeler Aligner (BWA) algorithm. Low-quality alignment and duplicate reads were removed by SAMtools. Standard MACS2 algorithm was used to call peaks, comparing matched treated and input samples, with a cutoff of P-value=1E-7. Peaks that were on the ENCODE blacklist of known false ChIP-Seq peaks were removed. Peaks called from multiple replicates were merged and only common peaks were used subsequently. Seqplots (Stempor and Ahringer, 2016) was used to generate heatmaps. Peaks were visualized by Integrative Genomics Viewer (IGV).

Differential binding events analysis between E14.5 and adult samples were statistically determined by DESeq2 (Love et al., 2014) using individual BAM files. The program normalizes the counts between samples using the median of ratio methods and calculates log2 fold-changes, shrunken-log2FC, P-value and adjusted P-value for each merged region. Genes associated with Vsx2 peaks were called if one or more peaks were present within 10 kb upstream or downstream of a given gene.

HOMER and GREAT analyses

HOMER enrichment motif analysis was run with standard settings with repeat masking on. The 200 bp surrounding the summit of peaks were analyzed. GREAT analysis was carried out using mm10 (mouse) or hg38 (human) with default parameters.

Acknowledgements

We are grateful to Susana da Silva for sharing Stagia3 plasmids and the AP protocol, and to Nathan Clark for sharing the mole acceleration track. We acknowledge the Health Sciences Genomics Research Cores at the University of Pittsburgh and the Magee-Women's Research Institute's Genome Editing, Transgenic, and Virus (GETV) Core Facility. We thank the Genome Engineering and iPSC Center (GEiC) at Washington University in St Louis for gRNA validation services. This research was also supported in part by the University of Pittsburgh Center for Research Computing through the resources provided and by the National Institutes of Health (core grant P30 EY08098 to the Department of Ophthalmology).

Competing interests

The authors declare no competing or financial interests.

Author contributions

Conceptualization: F.B., I.A.; Methodology: F.B., M.D., F.L., S.L., J.M.G.; Formal analysis: F.B., M.D., F.L., S.L.; Investigation: F.B., M.D., F.L., S.L.; Data curation: S.L.; Writing - original draft: F.B., I.A.; Supervision: J.M.G., I.A.; Funding acquisition: S.L., J.M.G., I.A.

Funding

This work was funded by a Research to Prevent Blindness career development award, by the National Institutes of Health (R01 EY030861-01A1), by a University of Pittsburgh start-up fund for I.A., and by the National Institutes of Health (R01 EY029031) for J.M.G. This research was also supported by the Eye and Ear Foundation of Pittsburgh and by an unrestricted grant from Research to Prevent Blindness. Deposited in PMC for release after 12 months.

Data availability

The sequencing data have been deposited in GEO under accession number GSE196106.

References

Aldiri, I., Xu, B., Wang, L., Chen, X., Hiler, D., Griffiths, L., Valentine, M., Shirinifard, A., Thiagarajan, S., Sablauer, A. et al. (2017). The dynamic epigenetic landscape of the retina during development, reprogramming, and tumorigenesis. *Neuron* **94**, 550-568.e10. doi:10.1016/j.neuron.2017.04.022

Bar-Yosef, U., Abuelaish, I., Harel, T., Hendler, N., Ofir, R. and Birk, O. S. (2004). CHX10 mutations cause non-syndromic microphthalmia/ anophthalmia in Arab and Jewish kindreds. *Hum. Genet.* **115**, 302-309. doi:10.1007/s00439-004-1154-2

Bassett, E. A. and Wallace, V. A. (2012). Cell fate determination in the vertebrate retina. *Trends Neurosci.* **35**, 565-573. doi:10.1016/j.tins.2012.05.004

Billings, N. A., Emerson, M. M. and Cepko, C. L. (2010). Analysis of thyroid response element activity during retinal development. *PLoS ONE* **5**, e13739. doi:10.1371/journal.pone.0013739
Brzezinski, J. A. and Reh, T. A. (2015). Photoreceptor cell fate specification in vertebrates. *Development* **142**, 3263-3273. doi:10.1242/dev.127043
Brzezinski, J. A. T., Lamba, D. A. and Reh, T. A. (2010). Blimp1 controls photoreceptor versus bipolar cell fate choice during retinal development. *Development* **137**, 619-629. doi:10.1242/dev.043968
Buecker, C. and Wysocka, J. (2012). Enhancers as information integration hubs in development: lessons from genomics. *Trends Genet.* **28**, 276-284. doi:10.1016/j.tig.2012.02.008
Burmeister, M., Novak, J., Liang, M.-Y., Basu, S., Ploder, L., Hawes, N. L., Vidgen, D., Hoover, F., Goldman, D., Kalnins, V. I. et al. (1996). Ocular retardation mouse caused by Chx10 homeobox null allele: impaired retinal progenitor proliferation and bipolar cell differentiation. *Nat. Genet.* **12**, 376-384. doi:10.1038/ng0496-376
Cepko, C. L., Austin, C. P., Yang, X., Alexiades, M. and Ezzeddine, D. (1996). Cell fate determination in the vertebrate retina. *Proc. Natl. Acad. Sci. USA* **93**, 589-595. doi:10.1073/pnas.93.2.589
Chen, Y., Chen, Y., Jastrzebska, B., Golczak, M., Gulati, S., Tang, H., Seibel, W., Li, X., Jin, H., Han, Y. et al. (2018). A novel small molecule chaperone of rod opsin and its potential therapy for retinal degeneration. *Nat. Commun.* **9**, 1976. doi:10.1038/s41467-018-04261-1
Cherry, T. J., Yang, M. G., Harmin, D. A., Tao, P., Timms, A. E., Bauwens, M., Allikmets, R., Jones, E. M., Chen, R., De Baere, E. et al. (2020). Mapping the cis-regulatory architecture of the human retina reveals noncoding genetic variation in disease. *Proc. Natl. Acad. Sci. USA* **117**, 9001-9012. doi:10.1073/pnas.1922501117
Clark, A. M., Yun, S., Veien, E. S., Wu, Y. Y., Chow, R. L., Dorsky, R. I. and Levine, E. M. (2008). Negative regulation of Vsx1 by its paralog Chx10/Vsx2 is conserved in the vertebrate retina. *Brain Res.* **1192**, 99-113. doi:10.1016/j.brainres.2007.06.007
Clovis, Y. M., Seo, S. Y., Kwon, J.-S., Rhee, J. C., Yeo, S., Lee, J. W., Lee, S. and Lee, S.-K. (2016). Chx10 consolidates V2a interneuron identity through two distinct gene repression modes. *Cell Rep.* **16**, 1642-1652. doi:10.1016/j.celrep.2016.06.100
Daghsni, M. and Aldiri, I. (2021). Building a mammalian retina: an eye on chromatin structure. *Front. Genet.* **12**, 775205. doi:10.3389/fgene.2021.775205
de Laat, W. and Duboule, D. (2013). Topology of mammalian developmental enhancers and their regulatory landscapes. *Nature* **502**, 499-506. doi:10.1038/nature12753
de Melo, J., Clark, B. S. and Blackshaw, S. (2016). Multiple intrinsic factors act in concert with Lhx2 to direct retinal gliogenesis. *Sci. Rep.* **6**, 32757. doi:10.1038/srep32757
Dennis, G., Jr, Sherman, B. T., Hosack, D. A., Yang, J., Gao, W., Lane, H. C. and Lempicki, R. A. (2003). DAVID: database for annotation, visualization, and integrated discovery. *Genome Biol.* **4**, P3. doi:10.1186/gb-2003-4-5-p3
Dorval, K. M., Bobechko, B. P., Fujieda, H., Chen, S., Zack, D. J. and Bremner, R. (2006). CHX10 targets a subset of photoreceptor genes. *J. Biol. Chem.* **281**, 744-751. doi:10.1074/jbc.M509470200
Emerson, M. M. and Cepko, C. L. (2011). Identification of a retina-specific Otx2 enhancer element active in immature developing photoreceptors. *Dev. Biol.* **360**, 241-255. doi:10.1016/j.ydbio.2011.09.012
Farhy, C., Elgart, M., Shapira, Z., Oron-Karni, V., Yaron, O., Menuchin, Y., Rechavi, G. and Ashery-Padan, R. (2013). Pax6 is required for normal cell-cycle exit and the differentiation kinetics of retinal progenitor cells. *PLoS ONE* **8**, e76489. doi:10.1371/journal.pone.0076489
Ferda Percin, E., Ploder, L. A., Yu, J. J., Arici, K., Horsford, D. J., Rutherford, A., Bapat, B., Cox, D. W., Duncan, A. M. V., Kalnins, V. I. et al. (2000). Human microphthalmia associated with mutations in the retinal homeobox gene CHX10. *Nat. Genet.* **25**, 397-401. doi:10.1038/78071
Fossat, N., Le Greneur, C., Beby, F., Vincent, S., Godement, P., Chatelain, G. and Lamonerie, T. (2007). A new GFP-tagged line reveals unexpected Otx2 protein localization in retinal photoreceptors. *BMC Dev. Biol.* **7**, 122. doi:10.1186/1471-213X-7-122
Goodson, N. B., Kaufman, M. A., Park, K. U. and Brzezinski, J. A. T. (2020a). Simultaneous deletion of Prdm1 and Vsx2 enhancers in the retina alters photoreceptor and bipolar cell fate specification, yet differs from deleting both genes. *Development* **147**, dev190272. doi:10.1242/dev.190272
Goodson, N. B., Park, K. U., Silver, J. S., Chiodo, V. A., Hauswirth, W. W. and Brzezinski, J. A. T. (2020b). Prdm1 overexpression causes a photoreceptor fate-shift in nascent, but not mature, bipolar cells. *Dev. Biol.* **464**, 111-123. doi:10.1016/j.ydbio.2020.06.003
Green, E. S., Stubbs, J. L. and Levine, E. M. (2003). Genetic rescue of cell number in a mouse model of microphthalmia: interactions between Chx10 and G1-phase cell cycle regulators. *Development* **130**, 539-552. doi:10.1242/dev.00275
Hartl, D., Krebs, A. R., Jüttner, J., Roska, B. and Schübeler, D. (2017). Cis-regulatory landscapes of four cell types of the retina. *Nucleic Acids Res.* **45**, 11607-11621. doi:10.1093/nar/gkx923
Heinz, S., Benner, C., Spann, N., Bertolino, E., Lin, Y. C., Laslo, P., Cheng, J. X., Murre, C., Singh, H. and Glass, C. K. (2010). Simple combinations of lineage-determining transcription factors prime cis-regulatory elements required for macrophage and B cell identities. *Mol. Cell* **38**, 576-589. doi:10.1016/j.molcel.2010.05.004
Honnell, V., Norrie, J. L., Patel, A. G., Ramirez, C., Zhang, J., Lai, Y.-H., Wan, S. and Dyer, M. A. (2022). Identification of a modular super-enhancer in murine retinal development. *Nat. Commun.* **13**, 253. doi:10.1038/s41467-021-27924-y
Horsford, D. J., Nguyen, M.-T. T., Sellar, G. C., Kothary, R., Arnheiter, H. and McInnes, R. R. (2005). Chx10 repression of Mitf is required for the maintenance of mammalian neuroretinal identity. *Development* **132**, 177-187. doi:10.1242/dev.01571
Housset, M., Samuel, A., Ettaiche, M., Bemelmans, A., Beby, F., Billon, N. and Lamonerie, T. (2013). Loss of Otx2 in the adult retina disrupts retinal pigment epithelium function, causing photoreceptor degeneration. *J. Neurosci.* **33**, 9890-9904. doi:10.1523/JNEUROSCI.1099-13.2013
Hughes, A. E. O., Myers, C. A. and Corbo, J. C. (2018). A massively parallel reporter assay reveals context-dependent activity of homeodomain binding sites in vivo. *Genome Res.* **28**, 1520-1531. doi:10.1101/gr.231886.117
Jadhav, A. P., Roesch, K. and Cepko, C. L. (2009). Development and neurogenic potential of Muller glial cells in the vertebrate retina. *Prog. Retin. Eye Res.* **28**, 249-262. doi:10.1016/j.preteyeres.2009.05.002
Javed, A., Mattar, P., Lu, S., Kruczek, K., Kloc, M., Gonzalez-Cordero, A., Bremner, R., Ali, R. R. and Cayouette, M. (2020). Pou2f1 and Pou2f2 cooperate to control the timing of cone photoreceptor production in the developing mouse retina. *Development* **147**, dev188730. doi:10.1242/dev.188730
Katoh, K., Omori, Y., Onishi, A., Sato, S., Kondo, M. and Furukawa, T. (2010). Blimp1 suppresses Chx10 expression in differentiating retinal photoreceptor precursors to ensure proper photoreceptor development. *J. Neurosci.* **30**, 6515-6526. doi:10.1523/JNEUROSCI.0771-10.2010
Kim, D. S., Matsuda, T. and Cepko, C. L. (2008). A core paired-type and POU homeodomain-containing transcription factor program drives retinal bipolar cell gene expression. *J. Neurosci.* **28**, 7748-7764. doi:10.1523/JNEUROSCI.0397-08.2008
Kim, S., Yu, N.-K. and Kaang, B.-K. (2015). CTCF as a multifunctional protein in genome regulation and gene expression. *Exp. Mol. Med.* **47**, e166. doi:10.1038/emm.2015.33
Koike, C., Nishida, A., Ueno, S., Saito, H., Sanuki, R., Sato, S., Furukawa, A., Aizawa, S., Matsuo, I., Suzuki, N. et al. (2007). Functional roles of Otx2 transcription factor in postnatal mouse retinal development. *Mol. Cell. Biol.* **27**, 8318-8329. doi:10.1128/MCB.01209-07
Kwan, K. M., Fujimoto, E., Grabher, C., Mangum, B. D., Hardy, M. E., Campbell, D. S., Parant, J. M., Yost, H. J., Kanki, J. P. and Chien, C.-B. (2007). The Tol2kit: a multisite Gateway-based construction kit for Tol2 transposon transgenesis constructs. *Dev Dynam* **236**, 3088-3099. doi:10.1002/dvdy.21343
Lee, J., Lee, H. J., Shin, M. K. and Ryu, W. S. (2004). Versatile PCR-mediated insertion or deletion mutagenesis. *Biotechniques* **36**, 398. doi:org/10.2144/04363BM04
Liu, I. S., Chen, J.-D., Ploder, L., Vidgen, D., van der Kooy, D., Kalnins, V. I. and McInnes, R. R. (1994). Developmental expression of a novel murine homeobox gene (Chx10): evidence for roles in determination of the neuroretina and inner nuclear layer. *Neuron* **13**, 377-393. doi:10.1016/0896-6273(94)90354-9
Liu, X., Feng, B., Vats, A., Tang, H., Seibel, W., Swaroop, M., Tawa G., Zheng, W., Byrne, L., Schurdak, M. et al. (2020). Pharmacological clearance of misfolded rhodopsin for the treatment of RHO-associated retinitis pigmentosa. *FASEB J.* **34**, 10146-10167. doi:10.1096/fj.202000282R
Livesey, F. J. and Cepko, C. L. (2001). Vertebrate neural cell-fate determination: lessons from the retina. *Nat. Rev. Neurosci.* **2**, 109-118. doi:10.1038/35053522
Livne-Bar, I., Pacal, M., Cheung, M. C., Hankin, M., Trogadis, J., Chen, D., Dorval, K. M. and Bremner, R. (2006). Chx10 is required to block photoreceptor differentiation but is dispensable for progenitor proliferation in the postnatal retina. *Proc. Natl. Acad. Sci. USA* **103**, 4988-4993. doi:10.1073/pnas.0600083103
Love, M. I., Huber, W. and Anders, S. (2014). Moderated estimation of fold change and dispersion for RNA-seq data with DESeq2. *Genome Biol.* **15**, 550. doi:10.1186/s13059-014-0550-8
Mao, C.-A., Wang, S. W., Pan, P. and Klein, W. H. (2008). Rewiring the retinal ganglion cell gene regulatory network: Neurod1 promotes retinal ganglion cell fate in the absence of Math5. *Development* **135**, 3379-3388. doi:10.1242/dev.024612
McLean, C. Y., Bristor, D., Hiller, M., Clarke, S. L., Schaar, B. T., Lowe, C. B., Wenger, A. M. and Bejerano, G. (2010). GREAT improves functional interpretation of cis-regulatory regions. *Nat. Biotechnol.* **28**, 495-501. doi:10.1038/nbt.1630
Merkenschlager, M. and Nora, E. P. (2016). CTCF and Cohesin in genome folding and transcriptional gene regulation. *Annu. Rev. Genom. Hum. G.* **17**, 17-43. doi:10.1146/annurev-genom-083115-022339
Mikkola, I., Bruun, J.-A., Holm, T. and Johansen, T. (2001). Superactivation of Pax6-mediated transactivation from paired domain-binding sites by dna-independent recruitment of different homeodomain proteins. *J. Biol. Chem.* **276**, 4109-4118. doi:10.1074/jbc.M008882200

Mills, T. S., Eliseeva, T., Bersie, S. M., Randazzo, G., Nahreini, J., Park, K. U. and Brzezinski, J. A. T. (2017). Combinatorial regulation of a Blimp1 (Prdm1) enhancer in the mouse retina. *PLoS ONE* **12**, e0176905. doi:10.1371/journal.pone.0176905

Murphy, D. P., Hughes, A. E. O., Lawrence, K. A., Myers, C. A. and Corbo, J. C. (2019). Cis-regulatory basis of sister cell type divergence in the vertebrate retina. *eLife* **8**, e48216. doi:10.7554/eLife.48216

Nishida, A., Furukawa, A., Koike, C., Tano, Y., Aizawa, S., Matsuo, I. and Furukawa, T. (2003). Otx2 homeobox gene controls retinal photoreceptor cell fate and pineal gland development. *Nat. Neurosci.* **6**, 1255-1263. doi:10.1038/nn1155

Norrie, J. L., Lupo, M. S., Xu, B., Al Diri, I., Valentine, M., Putnam, D., Griffiths, L., Zhang, J., Johnson, D., Easton, J. et al. (2019). Nucleome dynamics during retinal development. *Neuron* **104**, 512-528.e11. doi:10.1016/j.neuron.2019.08.002

Partha, R., Chauhan, B. K., Ferreira, Z., Robinson, J. D., Lathrop, K., Nischal, K. K., Chikina, M. and Clark, N. L. (2017). Subterranean mammals show convergent regression in ocular genes and enhancers, along with adaptation to tunneling. *eLife* **6**, e25884. doi:10.7554/eLife.25884

Pennacchio, L. A., Bickmore, W., Dean, A., Nobrega, M. A. and Bejerano, G. (2013). Enhancers: five essential questions. *Nat. Rev. Genet.* **14**, 288-295. doi:10.1038/nrg3458

Philips, G. T., Stair, C. N., Young Lee, H., Wroblewski, E., Berberoglu, M. A., Brown, N. L. and Mastick, G. S. (2005). Precocious retinal neurons: Pax6 controls timing of differentiation and determination of cell type. *Dev. Biol.* **279**, 308-321. doi:10.1016/j.ydbio.2004.12.018

Phillips, M. J., Perez, E. T., Martin, J. M., Reshel, S. T., Wallace, K. A., Capowski, E. E., Singh, R., Wright, L. S., Clark, E. M., Barney, P. M. et al. (2014). Modeling human retinal development with patient-specific induced pluripotent stem cells reveals multiple roles for visual system homeobox 2. *Stem Cells* **32**, 1480-1492. doi:10.1002/stem.1667

Reichman, S., Kalathur, R. K., Lambard, S., Ait-Ali, N., Yang, Y., Lardenois, A., Ripp, R., Poch, O., Zack, D. J., Sahel, J. A. et al. (2010). The homeobox gene CHX10/VSX2 regulates RdCVF promoter activity in the inner retina. *Hum. Mol. Genet.* **19**, 250-261. doi:10.1093/hmg/ddp484

Rowan, S. and Cepko, C. L. (2004). Genetic analysis of the homeodomain transcription factor Chx10 in the retina using a novel multifunctional BAC transgenic mouse reporter. *Dev. Biol.* **271**, 388-402. doi:10.1016/j.ydbio.2004.03.039

Rowan, S. and Cepko, C. L. (2005). A POU factor binding site upstream of the Chx10 homeobox gene is required for Chx10 expression in subsets of retinal progenitor cells and bipolar cells. *Dev. Biol.* **281**, 240-255. doi:10.1016/j.ydbio.2005.02.023

Rowan, S., Chen, C.-M. A., Young, T. L., Fisher, D. E. and Cepko, C. L. (2004). Transdifferentiation of the retina into pigmented cells in ocular retardation mice defines a new function of the homeodomain gene Chx10. *Development* **131**, 5139-5152. doi:10.1242/dev.01300

Roy, A., de Melo, J., Chaturvedi, D., Thein, T., Cabrera-Socorro, A., Houart, C., Meyer, G., Blackshaw, S. and Tole, S. (2013). LHX2 is necessary for the maintenance of optic identity and for the progression of optic morphogenesis. *J. Neurosci.* **33**, 6877-6884. doi:10.1523/JNEUROSCI.4216-12.2013

Samuel, A., Housset, M., Fant, B. and Lamonerie, T. (2014). Otx2 ChIP-seq reveals unique and redundant functions in the mature mouse retina. *PLoS ONE* **9**, e89110. doi:10.1371/journal.pone.0089110

Sentmanat, M. F., Peters, S. T., Florian, C. P., Connelly, J. P. and Pruett-Miller, S. M. (2018). A survey of validation strategies for CRISPR-Cas9 editing. *Sci. Rep.* **8**, 1-8. doi:10.1038/s41598-018-19441-8

Slattery, M., Riley, T., Liu, P., Abe, N., Gomez-Alcala, P., Dror, I., Zhou, T., Rohs, R., Honig, B., Bussemaker, H. J.et al. (2011). Cofactor binding evokes latent differences in DNA binding specificity between Hox proteins. *Cell* **147**, 1270-1282. doi:10.1016/j.cell.2011.10.053

Slavotinek, A. M. (2011). Eye development genes and known syndromes. *Mol. Genet. Metab.* **104**, 448-456. doi:10.1016/j.ymgme.2011.09.029

Stempor, P. and Ahringer, J. (2016). SeqPlots - Interactive software for exploratory data analyses, pattern discovery and visualization in genomics. *Wellcome Open Res.* **1**, 14. doi:10.12688/wellcomeopenres.10004.1

Uribe, R. A. and Gross, J. M. (2007). Immunohistochemistry on cryosections from embryonic and adult zebrafish eyes. *CSH Protoc.* **2007**, pdb prot4779. doi:10.1101/pdb.prot4779

Vitorino, M., Jusuf, P. R., Maurus, D., Kimura, Y., Higashijima, S. and Harris, W. A. (2009). Vsx2 in the zebrafish retina: restricted lineages through derepression. *Neural Dev.* **4**, 14. doi:10.1186/1749-8104-4-14

Wang, S., Sengel, C., Emerson, M. M. and Cepko, C. L. (2014). A gene regulatory network controls the binary fate decision of rod and bipolar cells in the vertebrate retina. *Dev. Cell* **30**, 513-527. doi:10.1016/j.devcel.2014.07.018

West, E. R. and Cepko, C. L. (2022). Development and diversification of bipolar interneurons in the mammalian retina. *Dev. Biol.* **481**, 30-42. doi:10.1016/j.ydbio.2021.09.005

White, M. A., Kwasnieski, J. C., Myers, C. A., Shen, S. Q., Corbo, J. C. and Cohen, B. A. (2016). A simple grammar defines activating and repressing cis-regulatory elements in photoreceptors. *Cell Rep.* **17**, 1247-1254. doi:10.1016/j.celrep.2016.09.066

Williamson, K. A. and FitzPatrick, D. R. (2014). The genetic architecture of microphthalmia, anophthalmia and coloboma. *Eur. J. Med. Genet.* **57**, 369-380. doi:10.1016/j.ejmg.2014.05.002

Wilson, D., Sheng, G., Lecuit, T., Dostatni, N. and Desplan, C. (1993). Cooperative dimerization of paired class homeo domains on DNA. *Genes Dev.* **7**, 2120-2134. doi:10.1101/gad.7.11.2120

Zhen, Y. and Andolfatto, P. (2012). Methods to detect selection on noncoding DNA. *Methods Mol. Biol.* **856**, 141-159. doi:10.1007/978-1-61779-585-5_6

Zibetti, C., Liu, S., Wan, J., Qian, J. and Blackshaw, S. (2019). Epigenomic profiling of retinal progenitors reveals LHX2 is required for developmental regulation of open chromatin. *Commun. Biol.* **2**, 142. doi:10.1038/s42003-019-0375-9

Zou, C. and Levine, E. M. (2012). Vsx2 controls eye organogenesis and retinal progenitor identity via homeodomain and non-homeodomain residues required for high affinity DNA binding. *PLoS Genet.* **8**, e1002924. doi:10.1371/journal.pgen.1002924

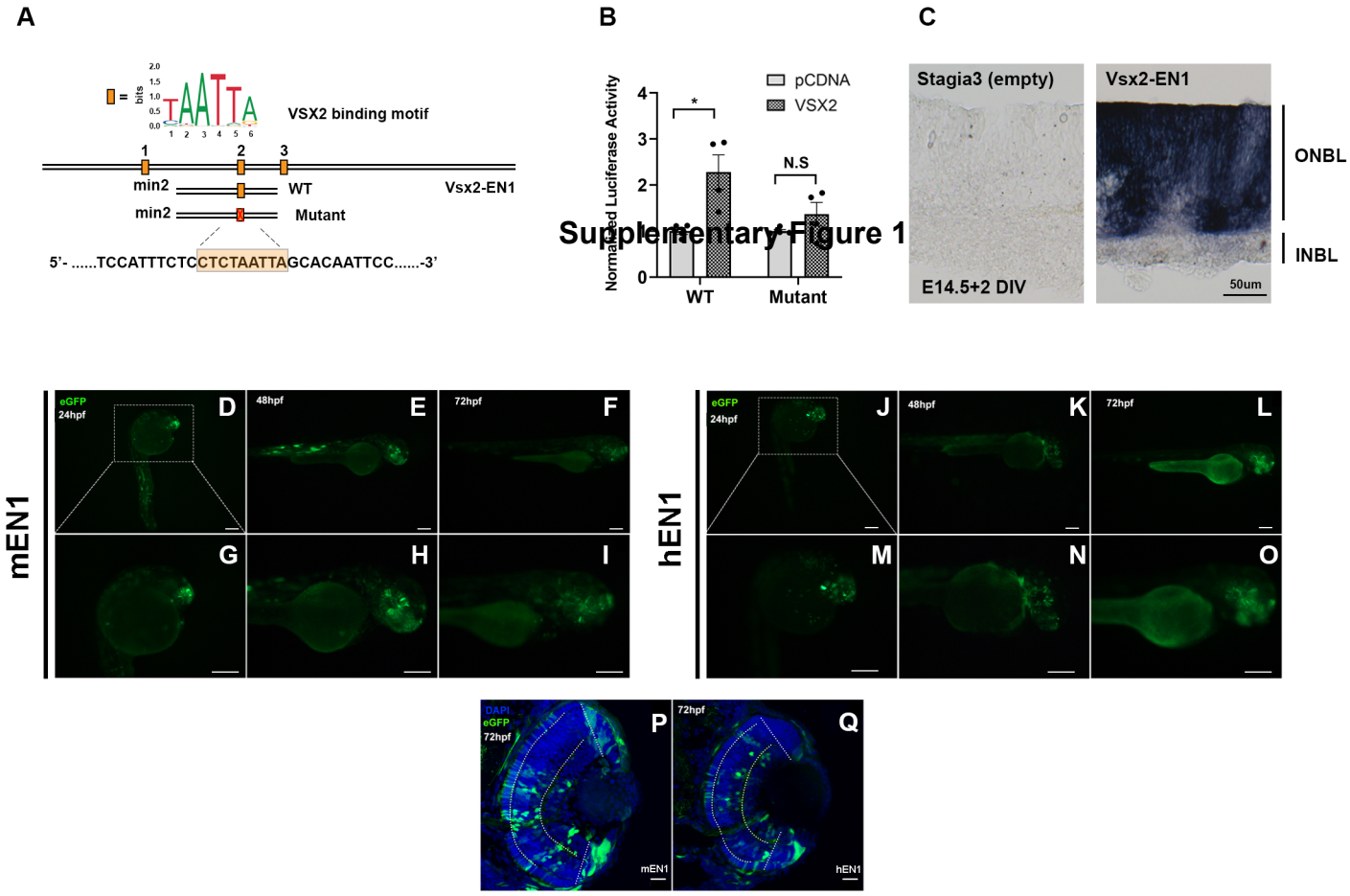

Fig. S1. A, Schematic showing the VSX2 predicted binding sites, min2 enhancer, and its deletion regions within the Vsx2-EN1. The highlighted sequence represents nucleotides that have been deleted. B, Luciferase assays of mouse min2 WT and min2 Mutant in the presence of VSX2. Data were shown as mean ± S.E.M, n = 4, P < 0.001 (***); P < 0.01 (**); P < 0.05 (*). C, AP staining in the cross-section of the retinas electroporated with empty or Vsx2-EN1 enhancer cloned in Stagia3 reporter construct. D- O, Whole-mount images of zebrafish embryos at the indicated stages after injection of mouse (D-I) and human (J-O) Vsx2-EN1 enhancer. P- Q, Cross sections of the developing zebrafish retina 72 hpf after injection with the constructs. Panels H, N and P are shown in the main figures.

Supplementary Figure 2

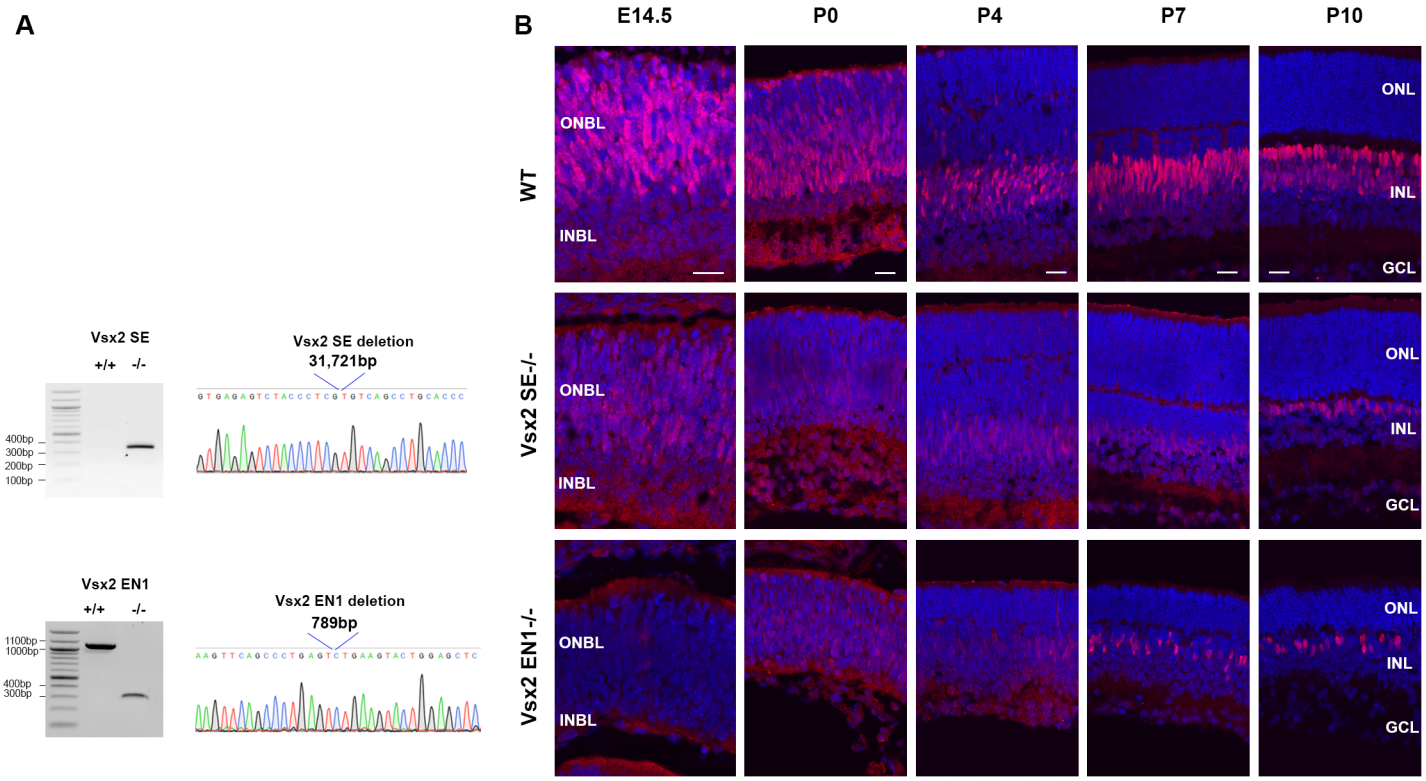

Fig. S2. A, Representative genotyping data (gel images of PCR products and sanger sequencing tracks) from Vsx2-EN1 and Vsx2-SE mouse lines. The deletion boundaries and sizes were indicated above each sequence track. B, Retinal cryosections at different developmental stages (E14.5, P0, P4, P7, P10) from WT, Vsx2-SE, and VSX2-EN1 deficient mice immunoassayed with VSX2 antibody.

Supplementary Figure 3

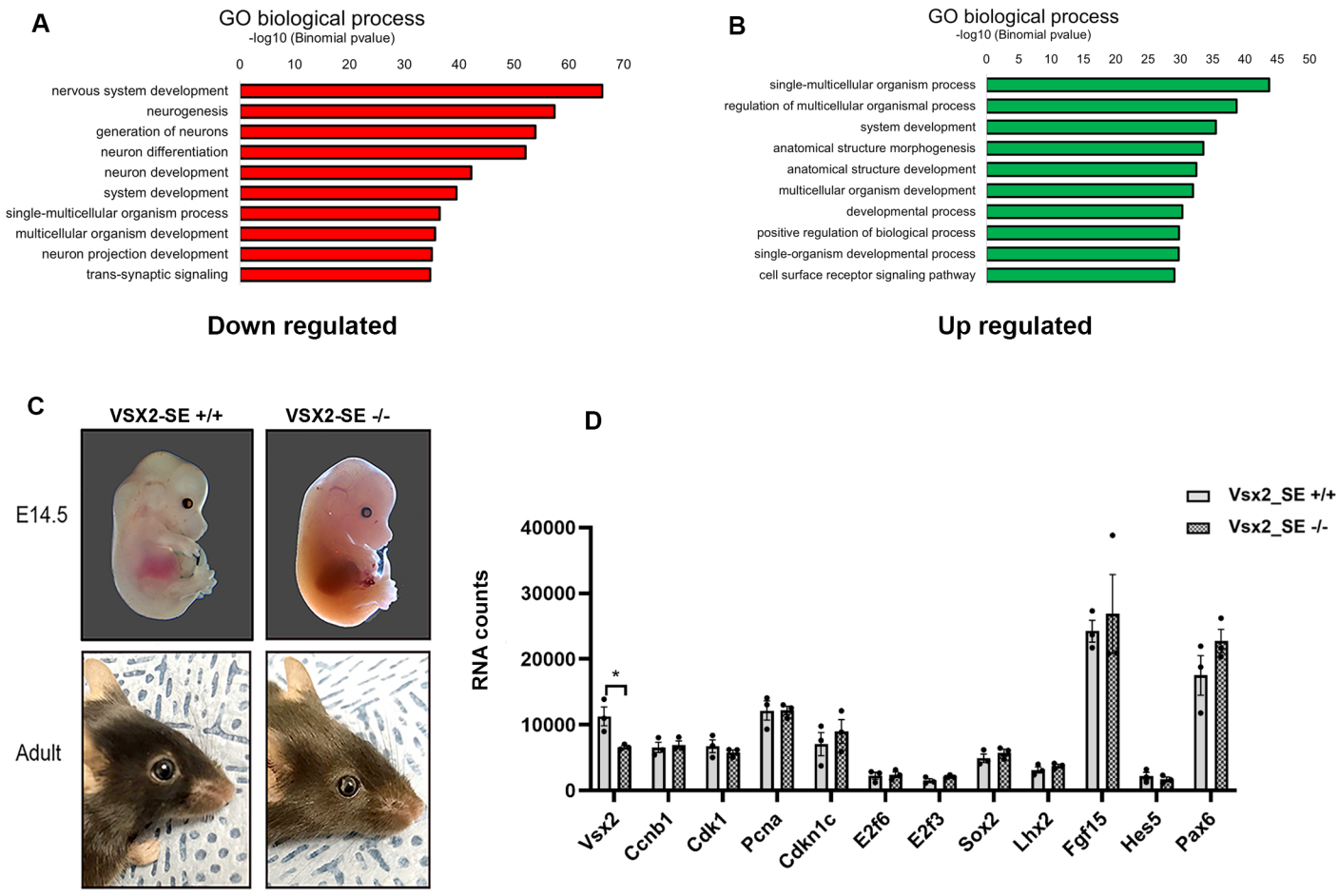

Fig. S3. A-B, Results of Gene Ontology (GO) enrichment analysis of downregulated (A) and up-regulated (B) genes in VSX2-EN1 KO mice at E14.5 retina. The lengths of the bars indicate the -log 10 -transformed P-values. Data were generated by Database for Annotation, Visualization, and Integrated Discovery (DAVID) software. C, VSX2-SE KO mice exhibit normal eye size compared to WT mice. D, Bar plot of RNA levels of selected RPC genes as determined by RNA-Seq analysis performed on VSX2-SE-/- and WT retinae at E14.5. Noticed that only Vsx2 is significantly downregulated.

Supplementary Figure 4

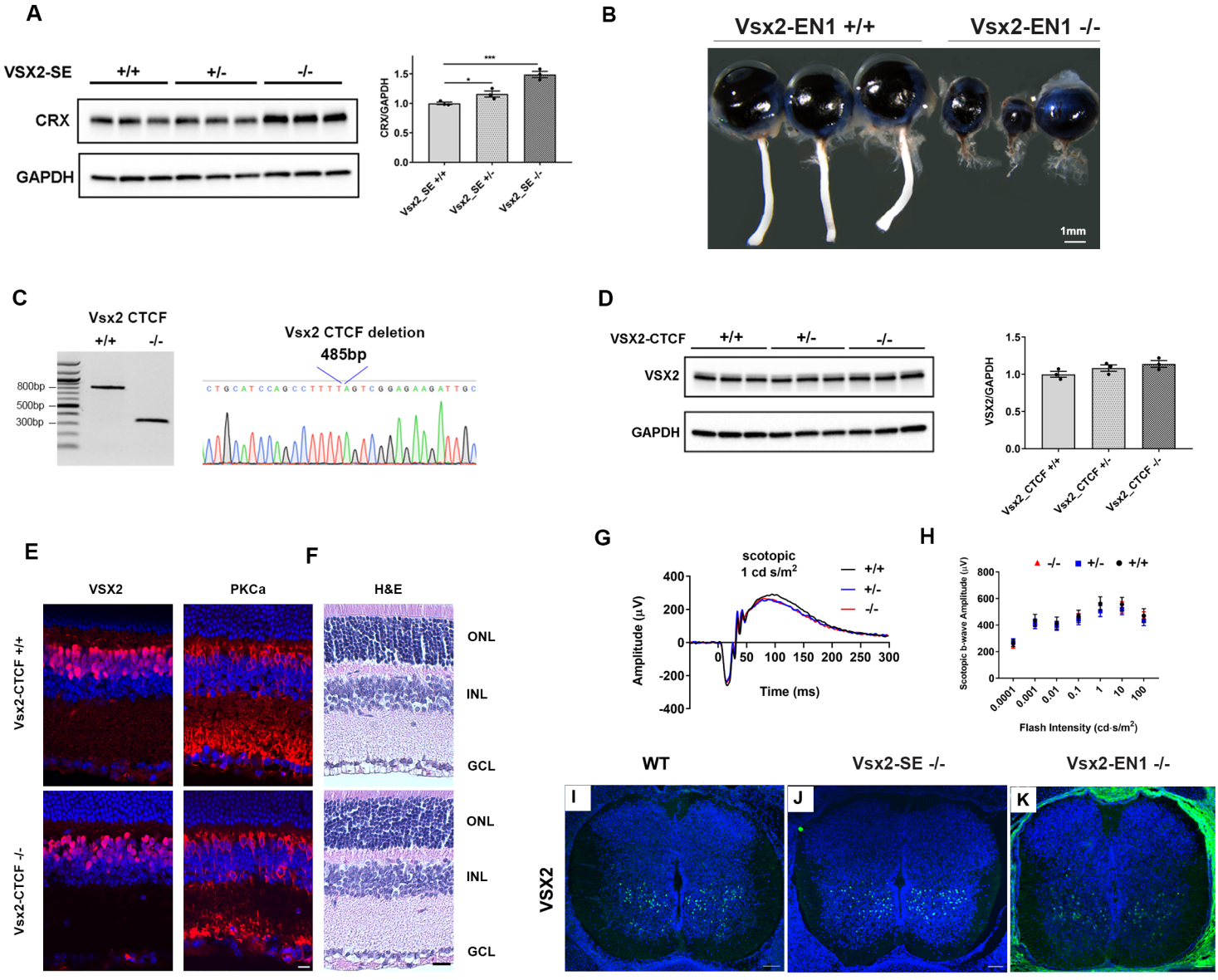

Fig. S4. A Western blot analyses of CRX performed on adult retinae from VSX2-SE-/-, heterozygous, and WT littermates with quantification. B, Adult eyes from VSX2-EN1 deficient mice are microphthalmic and exhibit optic nerve aplasia. C, Representative gel image of PCR products and sanger sequencing tracks from Vsx2-CTCF mouse lines. D, Analysis of *Vsx2* expression in adult *Vsx2*-CTCF-/-, heterozygous and WT littermates by Western blot with quantification. E, Immunohistochemistry of VSX2 and PKCa of the adult retina from *Vsx2*-CTCF-/- and littermate control. F, Hematoxylin and Eosin (H&E) staining of adult *Vsx2*-CTCF-/- retina and control littermates. G-H, ERG was recorded from different groups of mice at 6 weeks of age. Scotopic ERG responses from different groups of mice stimulated by a flash of light at 1 cd·s/m^2 (G) and plots of scotopic b- wave amplitudes (H) did not show any change in different groups (data were shown as mean ± S.E.M, $n = 3$, $P < 0.05$ (*)). I-K, Immunostaining of VSX2 on cryosections from WT (I), VSX2-SE-/- (J), and VSX2-EN1-/- (K) of the developing spinal cord at E14.5. Note that VSX2 remains expressed in the ventral spinal cord in VSX2 enhancer knockouts (scale bar 80 μm).

Table S1. Genomic coordinates (mm10) of VSX2 ChIP-Seq peaks in E14.5 and adult mouse retina

Click here to download Table S1

Table S2. Genomic coordinates (mm10) of VSX2 ChIP-Seq peaks near photoreceptors and bipolar genes in adult retina

Click here to download Table S2

Table S3. RNA-Seq data from VSX2-EN1 knockout retina at E14.5

Click here to download Table S3

Table S4. RNA-Seq data from VSX2-SE knockout retina at E14.5

Click here to download Table S4

Table S5. Genomic coordinates (hg38) of VSX2 ChIP-Seq peaks in adult human retina, and lists of photoreceptor and bipolar genes with VSX2 peaks

Click here to download Table S5

Table S6. Primer sequences for genotyping

Primer Name	Forward Primer 5′-3′	Reverse Prime 5′-3′	PCR size (bp)	
			no deletion	with deletion
VSX2-SE-homo	GCTCTGACCTTCCTGGAAGCCCGC	CTCAGGAGGTTACAAGGAGGTGTAG	none	300
VSX2-SE-Het	CATAACTGGCTGTATTCTGTGTGACTC	CTTACATCCTTTGACCCTGGCTATG	149	none
VSX2-EN1	GGCCAGGTAGGCCAAAGTAG	GTGTCGTACCTCAGTCACCG	1091	302
VSX2-CTCF	TGTGGCTCTCTGGAAGATGC	GGCGCGGAAATGAATGC	817	330

Table S7. Primer sequences for cloning

Name	Forward Primer	Reverse Primer
mVsx2	GCCGGATCCGCCACCATGACGGGGAAAGCGGGGGAAG	GCCTCTAGACTAAGCCATGTCCTCCAGCTG
mPAX6	GCCGGATCCGCCACCATGCAGAACAGTCACAGCGG	GCCTCTAGATTACTGTAATCGAGGCCAGTAC
hVsx2	GCCGGATCCGCCACCATGACGGGGAAAGCAGGGGAAG	GCCTCTAGACTAAGCCATGTCCTCCAGCTG
hPax6	GCCGGATCCGCCACCATGCAGAACAGTCACAGCGG	GCCTCTAGATTACTGTAATCTTGGCCAGT
mVsx2_En1	GCCGATATCCCTTCCCACCTTTTGTCTGGTA	GCCAAGCTTTGTGCTCGTCGAGGGTAGACT
mVsx2_En2	GCCGATATCCCCGGGCTTAGAGAGCATTT	GCCAAGCTTCAGGCACTTCCCAAGGAGAG
mVsx2_En1_min2_WT	GCCGATATCTTCTGCTTTGTCCCCCACCAGT	GCCAAGCTTAGGGAATGGCTCTCTTTGTAT
mVsx2_En1_min2_mutation	GTCCATTTCTCGCACAATTCC	GGAATTGTGCGAGAAATGGAC
hVsx2_En1	GCCGATATCTTGTCTATGCCTAAAGAGGCCA	GCCAAGCTTTTCTAGGGCAGAATTCACTCACG
hVsx2_En2	GCCGATATCGAGAAGCCTGAGGTTTAGCGATT	GCCAAGCTTCTCCACAAGCATGATCCTACTGA
mOTX2	GCCGGATCCGCCACCATGATGTCTTATCTAAAGCAACC	GCCTCTAGATCACAAAACCTGGAATTTCC
mPrdm1_En	GCCCTCGAGAGCCCTGACAAAGAGAGTGGGAG	GCCGATATCGTCGACACAAAAGCTGAGCTTTGAG

Table S8. Antibodies used in western blots and immunoprecipitation

Antibody	Company	Catalog number	Dilution
CRX	Santa Cruz	Sc-377207	1:500
GAPDH	ThermoFisher	MA5-15738	1:1000
PRDM1	Santa Cruz	SC47732X	1:500
PAX6	Active Motif	61611	1:1000 (3 µl in IP)
PAX6	Santa Cruz	Sc-81649	1:200
VSX2	Exalpha	X1180P	1:1000 (3 µl in IP)
VSX2	Santa Cruz	SC-365519X	1:1000
OTX2	R & D	AF 1979	1:1000 (3 µl in IP)

Table S9. Antibodies used in immunostaining

Antibody	Company	Catalog number	Dilution
PKCα	Santa Cruz	SC8393	1:100
SOX9	Millipore	AB5535	1:100
VSX2	Exalpha	X1180P	1:300
VSX2	Santa Cruz	SC-365519 X	1:500
Brn3a	Millipore	MAB1585	1/100
Calbindin	Sigma Aldrich	C9848	1/100
Cone Arrestin	Millipore	AB15282	1/300
Pax6	BioLegend	901302	1/300
Pax6	Active Motif	61611	1/300
Ki-67	Invitrogen	MA5-14520	1/100
OTX2	R & D	AF 1979	1:300